ASSESSMENT OF AN IRON FORMATION DEPOSIT IN IKANGA AREA, KITUI COUNTY, SOUTH EASTERN KENYA

BY

D. LAWRENCE BHOLLAI

I56/69084/2011

A DISSERTATION SUBMITTED IN PARTIAL FULFILLMENT FOR THE AWARD OF MASTERS OF SCIENCE DEGREE IN GEOLOGY (MINERAL EXPLORATION)

DECEMBER 5, 2013

UNIVERSITY OF NAIROBI

DECLARATION

This Dissertation is my original work and has not been presented for a degree in any other university.

D. Lawrence Bhollai ---------- ----------
I56/69084/2011 Signature Date

This Dissertation has been submitted for examination with the approval of my supervisors:

Dr. Christopher M. Nyamai ---------- ----------
Signature Date

Dr. Daniel W. Ichang'i ---------- ----------
Signature Date

UNIVERSITY OF NAIROBI

DECLARATION FORM FOR STUDENTS

Declaration of Originality Form

This form must be completed and signed for all works submitted to the University for examination.

Name of Student: Lawrence Bhollai Duo

Registration Number: I56/69084/2011

College: College of Biological & Physical Sciences

Faculty/School/Institute/Department: Department of Geology

Course Name: Master of Science in Geology (Mineral Exploring)

Title of the work: Assessment of an iron formation deposit in Ikanga Area, Kitui County, South Eastern Kenya.

DECLARATION

I understand what Plagiarism is and I am aware of the University's policy in this regard I declare that this **Dissertation project** is my original work and has not been submitted elsewhere for examination, award of a degree or publication. Where other people's work or my own work has been used, this has properly been acknowledged and referenced in accordance with the University of Nairobi's requirements. I have not sought or used the services of any professional agencies to produce this work. I have not allowed, and shall not allow anyone to copy my work with the intention of passing it off as his/her own work. I understand that any false claim in respect of this work shall result in disciplinary action, in accordance with University Plagiarism Policy.

Signature:_____

Date: _____

ABSTRACT

This Research was conducted in the Ikanga area, which occurs at the intersection of longitude 38º33'50''E and latitude 1.7º25'45'' S in Kitui County, south-eastern Kenya. The Area lies within the Neoproterozoic Mozambique Belt in which the iron formation deposit, which is the main focus of this study occurs. The deposit is, approximately 250km away from the city of Nairobi. This study was conducted purposely to assess the iron formation deposit in the Ikanga area and find out whether it has some economic value or not. The area is a gently low undulating semi-arid land with acacia tree family and dry drainage system. The rock types of the area are Neoproterozoic in age and include granitoid gneisses which are dominant. On the local scale, granitoid, feldspathic gneisses, kunkar limestone, migmatite, lateritic-silica-baked-ferrous-canga and marble do occur. Alluvial sandy soil deposits of Pleistocene and Recent Age, which include red and black soils, form the local geology of the study area. In pursuance of this research, the following methods were applied: 1). Remote Sensing; 2). Ground Magnetic Survey; 3). Geochemical Analysis; 4). Mineralogical and Petrographical Analyses; and 5). Data Analysis using Software Applications. Application of these methods showed varied results. Remote sensing gave a broad pictorial view of the study area and its surroundings and identified where the iron formation deposit is concentrated for favorable sampling point sections prior to the field work. The Landsat Band etm+3:1 ratio for iron oxide displayed the dispersion of the iron formation in the study area. The ground magnetic method was able to determine the magnetic fields of the area. A proton precision magnetometer was employed in this geophysical mapping to collect total magnetic field in the area. Analysis of the total magnetic intensity (TMI) of the area and associated magnetic source results mark the locations and orientations of southwest-northeast trending linear structures at depth caused by shearing and subsequent mineral alterations. The areas occupied by magnetic highs to the east are interpreted to coincide with locations of iron formations and require ground follow-up and truthing. Geochemical data analyses confirmed predominantly oxide facies mineralization with Fe_2O_3 as the main iron oxide. The highest non-iron oxide amounts in the domain include TiO_2 (≤9.72 wt% in the soil), MnO (≤ 0.2 wt% in haematite, gneiss, and soil), CaO (≤ 54.7 wt% in limestone), Al_2O_3 (≤ 21.8 wt% in soil), Na_2O (≤ 4.31 wt% in gneiss), K_2O (≤ 3.6 wt % in soil) and SiO_2 (≤ 83.63 wt% in pegmatites). The Fe_2O_3 wt% in the hematite mineralized samples ranges from 72.4% to 86.3% Fe_2O_3 wt% with an average of 76.97 Fe_2O_3 wt%. In gneisses the Fe_2O_3 wt% ranges from 3.38 to 16.4 wt%, with an average of 8.0 wt%, while in the soil the Fe_2O_3 wt% ranges from 3.9 to 79.6 wt%, with an average of 22.65 wt%. The geochemical data indicate that the Ikanga deposit is very likely to have been derived from a Precambrian Banded Iron Formation (BIF) precursor by the weathering processes.

DEDICATION

This dissertation is dedicated to all geoscientists for their continuing hard work in producing voluminous literature in geology from which fruits I have carried out this study. It is also dedicated to relatives and friends for their continued words of encouragement given to me during my stay at the University of Nairobi, and which provided me with partial strength to complete these postgraduate studies.

ACKNOWLEDGEMENTS

This study was made possible through the financial support from the Department of Geology, University of Liberia under the Chairmanship of Prof. Albert T. Chie, the Director of Fiscal Policy of the University of Liberia, Prof. Wilson Tarpeh, and the Comptroller Mr. Selhma Jallah. All of my sponsors and supervisors are duly acknowledged for their support in this study and for their continued commitment to scientific research. I would like to thank the Chairman of the Department of Geology, University of Nairobi, Dr. Christopher M. Nyamai mainly for helping to make my stay at the University of Nairobi a pleasant and rewarding one. The same feeling of gratitude is conveyed to the entire staff of the Department of Geology for their warm humanitarian reception, and academic guidance given to me during my stay (2011-2013) at the University of Nairobi. Dr. Christopher M. Nyamai, Dr. Daniel W. Ichang'i, and Mr. Aaron K. Waswa supervised this project and assisted me with tremendous help to me in giving technical and moral support to make the completion of this study a reality. I acknowledge them for their willingness and participation in the critical review of this dissertation. Mr. Aaron Waswa travelled with me to the field and greatly assisted me in the field work. His input in this study has been considerable and is much appreciated and memorable. My thanks also go to Mr. Samuel Mbiga for preparing petrographic thin sections and assisting in the analyses of samples and associated minerals. The assistance of dr. Nyamai and Dr. Ichang'i in the petrographical aspects of the study is very much appreciated. The assistance of Mr. Stanley Atonya on the ArcGIS graphical presentation in this study is acknowledged. Mr. Thomas Wanambisi is remembered and acknowledged for his time and patience in typing and arranging this work. All field maps and other materials used in this study were provided by the Department of Geology, University of Nairobi. This assistance is highly appreciated. Mr. Cosmas N. Mutune, really assisted me in the field work and the cooperation of the community leaders of Ikanga area made our stay in the field rewarding and very much indelible. I have also learned and enjoyed the companionship and support of other students in the Department of Geology. I wish to especially thank Yussuf Tsuma Mgutu for assisting me in the magnetic data analysis in this dissertation. My thanks and appreciations also go to the Mines and Geological Department of the Ministry of Mining, Republic of Kenya for the geochemical analyses of my samples. Finally and most important, I thank the Almighty God for giving me the strength and direction to complete this study.

TABLE OF CONTENTS

LIST OF FIGURES

LIST OF TABLES

LIST OF ABBREVIATIONS

DALP - Distance along Profiles

IGRF – International Geomagnetic Reference Field

nT - Nanotesta

SI - Structural Index (geological body in the subsurface formation)

UTM - Universal Traverse Mecator projected coordinate system

VDTIF - Vertical Distance to the Iron Formation Downward

CHAPTER ONE: INTRODUCTION

This research project was designed to assess the iron formation deposit in the Ikanga area, southeastern Kenya and to ascertain whether it has some economic value or not. The study area is low lying, with sparse vegetative cover and gently undulating soil profiles. The area has lateritic outcrops which form ferricrete capping in places consisting of composite units of gritty sandy materials. Well defined rock outcrops are not common. What are common in the study area are recent alluvial sedimentary deposits.

1.1 Introduction and General Information

Ths study focuses on a thinly scattered iron formation deposit in the regolith in the Ikanga area rather than the massive banded iron formation that are hosted in well defined lithologies in large concentrations. There is limited published data on the Ikanga type of regolithic iron deposit. Regolithic iron deposits in this sense actually represent low value, but readily accessible sources of iron. Until about some decades ago, such iron mineralization was considered uneconomic owing to the low iron content which was not sufficient to attract investors. With the increasing availability of effective and relatively less expensive metallurgical processes for the treatment of lateritic ores (Kennedy, 1989), this set of low grade deposits has become an economic source of iron and associated minerals, and is currently the focus of numerous exploration programmes in Australia, Africa, South Africa and India (Butt, 1988; Bowell et al., 1991; Davy and El-Ansary, 1989).

The Ikanga iron deposits were investigated using a combination of techniques. These included geological field mapping followed by petrographic analysis of rock samples. The ground magnetic geophysical mapping technique was employed to study this deposit. Magnetic data were acquired along fifteen profiles at the end of every twenty meter interval and the data obtained were analyzed and studied which indicated the various depths of the iron formation deposit in the study area, ranging from zero meters on the surface and to below meters beneath the surface. This mapping was conducted by the use of the proton magnetometer, also known as the proton precession magnetometer (PPM), which uses the principle of Earth's field nuclear magnetic resonance (EFNMR) to measure very small variations in the Earth's magnetic field, allowing ferrous objects on land and at sea to be

detected (Desa et al., 2007). Geochemical data were acquired and also analyzed to characterize the Fe composition of the Ikanga iron deposit and associated minerals.

This research project is presented in this dissertation in five chapters. Chapter One gives the introduction to this project, while Chapter Two presents the methodology and materials used. Chapter Three presents the information acquired during the field mapping and associated petrographic analysis phases. This chapter then discusses the geologic setting and mode of occurrence of the Ikanga iron deposit. Chapter Four presents the results of the ground magnetic survey of the Ikanga area and also the results of the geochemical analysis of samples from the project area. Chapter Five presents the discussion, conclusions and recommendations arising from this research project.

1.2 Problem Statement

The growth in global population and the increasing demands of man to construct shelters, build industries, and infrastructure in general, have made the use of iron ore products very much important. Development of communities and nations worldwide therefore requires the use of materials that are derived from iron ore productions. It is predicated upon this background that this research project is designed to assess and ascertain the Ikanga iron deposit to ascertain whether it has some economic values and whether this deposit can be utilized for the development of the Ikanga's Community and the Republic of Kenya at large. This project also seeks to provide information on the geological, geochemical, and geophysical information and data on the Ikanga iron deposit.

1.3 The Study Area

The study area lies in a geographical region centered on longitude $38^{0}33^{'}50^{''}$E and latitude $1.7^{0}25^{'}45^{''}$ S in Kitui County, south-eastern Kenya (Figure 1.1). A detailed description of the locality of the study area is further presented in a topographical map of Ikanga (Figure 1.2). The area is defined by its post Archaean, metamorphic rocks of north-south trending Mozambique mobile Belt of Neoproterozoic age consisting predominantly of granitoid gneisses and quartzo-feldspathic gneisses (Warden and Horkel (1984). The area also contains sedimentary deposits of Quaternary age. Walsh (1959) argued that the rocks in the study area are all of sedimentary in origin. Hornblende–biotite gneisses in the area are thought to represent a difference of composition in the original sediments, perhaps an increment of

chlorite, as compared with those sediments which gave rise to the hornblende gneisses, rather than a difference in metamorphic grade.

Figure 1.1 Showing the Ikanga study area outlined in red (modified after Rop (2011)).

1.3.1 Location and description of the study area

The study area can be defined by its four corner rectangular points which are presented in the UTM coordinates as: (391000E, 9817000N); (391000E, 9818000N): (394000E, 9817000N) and (394000, 9818000N) on the topographical map of Ikanga. The study area is 1km wide north-south and 3km long east-west and lies just to the west of the main road leading to Ikutha from Kitui Town via Ikanga, between Makaleh and Dakadede towns. It is approximately six kilometers (6km) to the north-north-west (NNW) of Ikanga (Figure 1.2). The north-south trending Nzeeu River, which is one of the main Rivers in the Ikanga area, crosscuts the study area into two parts (Figure 1.2). To the southwest of the study area also lies a floodplain. This floodplain comprises of alluvial sedimentary deposits, which have been transported by the flooding of the Nzeeu River during rainy seasons. Flooding serves as the

mechanisms through which heterogeneous surface soil materials are deposited in the study area.

In much of the study area the surface soils are reddish brown, and in some portions, the vegetation cover has been removed by overgrazing and poor animal husbandry. The fertile portion of the study area is along the western side of the Nzeeu River bank on which all agricultural activities are carried out. Kunkar limestones are widely developed in the area. They are usually buff or pink in color due to iron staining, and often include angular fragments of quartz and feldspars. These limestones seldom exceed a few meters in thickness.

The area is situated in the Neoproterozoic Mozambique Belt in which complex geological features occur in the Neoproterozoic rocks (Warden and Horkel (1984)). The metamorphic grade of the Neoproterozoic rocks in the study area shows characteristics of the almandine-diopside-hornblende subfacies of the amphibolite facies (Turner, 1948, pp.87-88). Differentiated alluvial deposits form part of the regolith. These deposits are the dominant sedimentary sources for much of the clastic sequences deposited during the Neogene (Feibel, 2011). They include buff-colored arkosic, channelized fluvial pebbly minor conglomeratic grits and exhibit a wide scatter of palaeocurrent directions to the west, north and east suggesting a generally northerly directed flow (Morley et al., 1992).

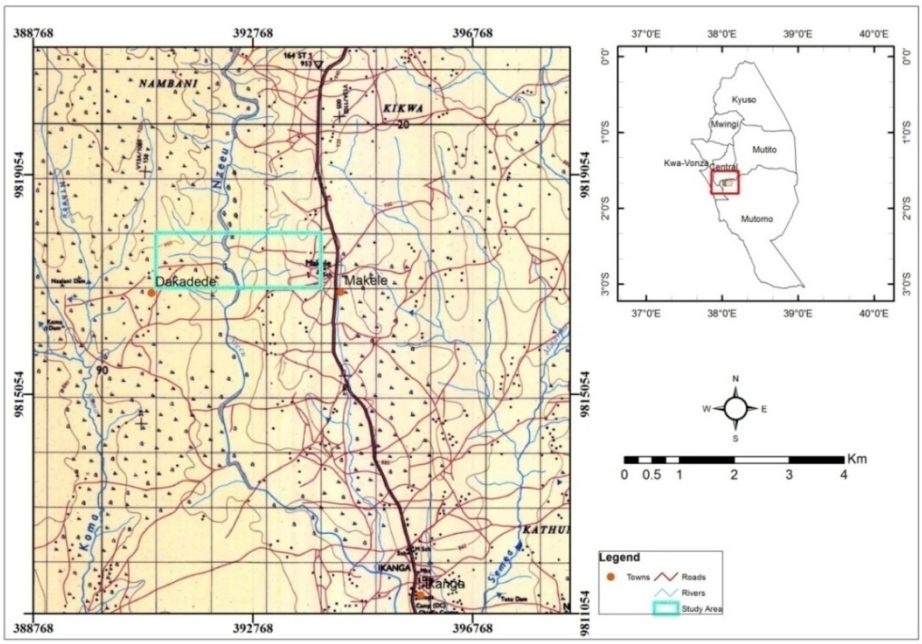

Figure 1.2 Topographical Map of Ikanga showing the location of the Study Area. Source: Directorate of Overseas Surveys (D.O.S) 423 (Series Y731), Edition I-D.O.S., Published by the Directorate of Oversea Surveys for the Kenya Government, Sheet 164/1 (1965).

1.4 Climate

The climatic conditions in the study area are varied. Annual rainfall patterns show a maximum in March-April-May and a lesser peak period in November-December. Like some parts of Kenya, the study area is a semi-arid region with daily temperature variation occurring between 24 and 38 degree Celsius. The rainfall ranges approximately between 120mm and 300mm per annum. At times the seasonal variations occur producing more and less cold and warming temperatures starting at the beginning, and also in the middle up to the end of the year. The dry season is the longest and has a negative effect on the plants and animals. One of the effects of less rain fall is that the soils are less fertile in natural nutrients and this causes the destruction of plants and animals. The long term dry season also creates dry river beds and channels. During this period, waters seep below the water table and leave behind dry river channels with no water. The western parts of the study area where there are low elevations receive more runoff during the rainy season and finally develop flourishing vegetation. The rains usually occur under the influence of the southeastern and northeastern Monsoons, which originates over the India Ocean and are relatively cool and moist and at times bring torrential rain. Further, the distribution of rains in the area is also controlled by the land masses and topography (Olang, 1979).

1.5 Vegetation

Vegetation in the study area mainly consists of scattered acacia bushes and a cover of herbaceous plants. The density of the acacia bushes increases in the peneplains. This pattern is repeated until it becomes invariant. The vegetation is therefore geologically controlled (Joubert, 1966). On the western side of the study area where there is a flood plain, the vegetations are classified as shrubs. Sparse bushes occur in parts of the area with thin soil cover and poor nutrients, especially in the highland areas to the east.

1.6 Land Use

The people in the study area can utilize the land in many applications depending on the needs of their livelihood. Generally, the land is mostly used for cattle grazing and agriculture activities. The land is also used to provide safe drinking water from hand dug wells. Agricultural activities are mostly concentrated in the lowland areas which comprise of nutrient alluvial deposits. These agricultural activities include: mellow farming; maize farming and mallet farming. Local bricks are also produced from the soils for construction purposes.

Due to the aridity conditions of the soils, only few plants are grown on the land such as; corns, melons, papaya, millet, carrots, hibiscus and creeping seed producing plants which include beans, etc. The most common food producing garden plants are maize. Typical farms (see Figure 1.3) are located in the low land areas within the floodplain of the north-south trending Nzeeu River. Oil producing plants like palms, cocoanuts, breadfruits, etc are not grown.

Figure 1.3 Field photograph showing a partial view of one of the maize farms visited in the project area at the time.

1.7 Physiography and Drainage

The physiographical overview of the study area is divided into two natural regions in which the types of relief and drainage patterns are varied. The floodplain to the west is one part of this physiography and is the low land areas. The second part of this physiography is the highland portion on the east which is higher in elevation than the floodplain areas. The north-south trending Nzeeu River in the study area is here referred as the major River on the erosion surface. However, during this study the Nzeeu River was dried in its beds. Streams in the study area are seasonal, not perennial. They can become dried during the dry season and flooded during the rainy season. On the surface of the study area gullies are developed in the regolith and are the channels for runoff through which sedimentary materials are transported to the lowland areas during the raining season. The entire study area is gently

undulating ranging from 600m to 1000m high. Tors of low angle limbs formed low level synclinal folding on the surface in which the soil erosions crosscut the tors crest orientations.

1.8 Literature Review

Iron formations have been classified on the basis of mineralogical composition (James, 1954). The tectonic setting of iron formation was also proposed by (Gross, 1965) and depositional environment by Kimberley (1978). The large variety of available classification schemes undoubtedly reflects our limited understanding of iron formation. According to James (1954), the original facies concept of iron formation included oxide-, silicate- and carbonate and that the facies iron formation thought to correspond to different water depths. A fourth so-called sulphide-facies, containing pyrite [FeS_2] and/or pyrrhotite [Fe_{1-x} S], was once regarded as being syngenetic in origin (Fripp, 1976) but has subsequently been suggested to be epigenetic (Phillips *et al.*, 1984; Groves *et al.*, 1987) with a replacement rather than primary sedimentary origin for sulphide mineralization.

Gross (1983) infers a tectonic setting of iron formation deposit on the basis of size and lithologic associations. He proposed that the *Algoma*-type iron formations are relatively small, and associated with volcanogenic rocks. Iron formation has a primary iron content that rarely exceeds 10^{10} tons (James and Trendall, 1982). Typical lateral extents are less than 10 km, with thicknesses in the range 10-100 m (Goodwin, 1973; Appel, 1980; Condie, 1981). Many workers have favored depositional environments for this type of iron formation to include island arc/back arc basins (Veizer, 1983) and intracratonic rift zones (Gross, 1983). Beukes (1973) provided a geological overview of Precambrian iron formations of the Southern Africa region. Beukes (1983) further discussed the paleoenvironmental setting of iron formations in the depositional basin of the Transvaal Supergroup in South Africa. Beukes and Klein (1992) provided models for iron formation.

Past field work in the Ikanga area has shown that pebbles of lava are found up to twenty four (24) kilometres (15miles) from the most prominent plateau across a watershed in the area west of Kitui Township (Schoemann, 1948, p.6), and that these pebbles are weathered from the exposed Precambrian rocks which are associated with the iron formation in Ikanga. Where hills are common particularly to the end of the Tertiary surface and on the pediment among the hills and sub-Miocene surface, the possibility of iron mineralization in those hills is common. These hills can take the form of tors and inselbergs and usually mark outcrops of

steeply-dipping strata that may probably serve as catchment for iron mineralization in the - study area (Walsh, 1959).

It has been reported from preliminary results of magnetic survey in the Nyanza area that several trends on the Kanga grid appear to be associated with large, and deformed iron formation, a mineralization type that is reported from the greenstone belt elsewhere in Kenya as well as in Tanzania (e.g. AngloGold, Ashanti's Geita and Barricks Golden Ridge Mine). Further to the Kwoyo grid, located to the northwest (NW) of Ikanga area, a ground follow-up of Au-As-Sb-Cu-Zn soil survey has also discovered a similar anomaly that is generally underlain by a large deformed iron formation sequence (Stockport Exploration, Nyanza Sotik Project overview, Kenya).These deposits may probably extend to the Research Area since they are adjacent and occur in the same Mozambique Belt. The section of the Neoproterozoic Mozambique Belt in which Ikanga is located in southeastern Kenya, where this research has been conducted is predominantly composed of remobilized and recrystallized Precambrian rocks. Among these rocks, some exhibit iron formation inclusions in their fabric and bedding **(**Warden and Horkel, 1984). More detailed geological accounts of part of the Neoproterozoic Mozambique Belt which underlies the study area are well treated by various reports and research papers documented by Nyamai (1999), Nyamai et al. (2003; 2000; 1999), Mathu (1992), Mathu and Tole (1984), Mathu et al. (1994), Saggerson (1957), Dodson (1953, 1955), Baker (1954), Sanders (1954), and Schoeman (1948). It has been documented by these authors that southern Kenya is comprised of an overlying Kurase- Kasigai Groups of sediments that show facies change eastwards from shallow water shelf lithofacies to deep water sediments which can be probably associated with sedimentary iron formations.

According to Dodson (1953), granitoid gneisses in the Neoproterozoic Mozambique Belt of Kenya contain magnetite. Biological mechanisms can potentially account for the precipitation of iron out of solution in a variety of environments, ranging from an oxygenic photic zone to a locally oxygenated sub-photic zone (Konhauser et al., 2002). Report by Van Straaten (1984), Kuhn et al. (1990), and Kuhn (1984) disclosed that during the emplacement of the Mozambique Belt, it was accompanied by mineralization fluids in which massive base metal sulphide and sedimentary iron formation deposit may have occurred. Iron formation deposits in the Mozambique Belt were probably formed from a hydrothermal vent system, but its distal position for now can be indicated by a very fine-grained laminated tuffs underlying and intercalated with the iron formation (Konhauser et al., 2002). Due to the increasing

availability of effective and relatively less expensive metallurgical processes for the treatment of lateritic ore deposits, such class of deposits can be treated to extract the needed iron metal (Kennedy, 1989).

The lateritic class of ore deposits similar to the Ikanga deposit has become an important source of gold, base metals, and iron formation in other parts of Africa, Australia, South Africa and India (Lyoon, 1957; Bowell el al., 1991; Davy and El-Ansary, 1989) and are now the focus of detailed exploration work. It is documented by Windley (1984) that early iron formations are about the same age on many continents, but reached their peak of development in the early Proterozoic basins or geosynclines near the boundary of the Archaean. The Mozambique Belt in which the Study Area is located, in Kenya is a Neoproterozoic Segment (Schlüter, 1997). The possibility of iron formations occurrence in Kenya is sure. The project area is located in the Neoproterozoic Mozambique Belt terrain and which, it is believed, probably contains some iron formations. Current work on the geochemical characterization of iron ore deposits of the Mozambique Belt in the Ikutha area, in the southern portion of the study area indicates the existence of iron ore bearing rocks consisting magnetite and hematite and including apatite and phosphate concentrations which are worth further exploration (Nyamai, 2013). The proximity of this research project area to where the current information has emerged of iron ore bearing rocks may very well indicate that such geological formations may extend beyond to form other deposits elsewhere and also in the research area.

1.9 The Main Objective of this Research Project

The main objective of this research project is to assess and ascertain the geologic nature of the Ikanga iron deposit and to ascertain whether it has some economic value and can be utilized for the development of the Ikanga Community and the Republic of Kenya in general.

1.10 Specific Objectives of this Research Project

The specific objectives of this research project are given below.

Specific Objective One (1):

The first objective is to collect geological, geochemical, and geophysical information and data on the Ikanga iron deposit in order to characterize its nature.

Specific Objective Two (2):

The second objective is to establish the geological setting, host rocks, composition, mode of occurrence and origin of the Ikanga iron deposit.

Specific Objective Three (3):

The third objective is to assess and ascertain whether the Ikanga iron deposit in the study area has economic value or not and to make appropriate recommendations.

1.11 The Research Question of this Project

How does the Ikanga iron deposit occur in the study area, and what relationship does it have with pre-existing iron formations ?.

1.12 Justification and Significance of the Research Project.

Iron is globally the predominant metal in the constructions and manufacturing industries. The ore from which iron is derived is the geological material that can be extracted from beneath the surface and exploited for benefit of man. In this research project the Ikanga iron deposit is investigated to ascertain and whether it has potential for economic value and whether this deposit can, therefore, be utilized, and if so, what approach should be followed in the utilization of this resource in future.

CHAPTER TWO: METHODOLOGY AND MATERIALS

In order to achieve the objectives of this research project, the following methods, approaches, materials, and software were applied in addressing the research question for this project.

2.1 Remote Sensing Method

Remote sensing was used in this study to show a broad pictorial view of the study area and to identify areas in which the iron deposit is concentrated before the start of the field work. The basic concept is to enhance recognition of the areas of concentration in the study area and surroundings, for better planning of the field work and for optimal selection of sampling sites.

2.2 Geological Field Mapping, Sampling and Data Collection

Geological field mapping and sample collection of rock and iron rich samples in the Ikanga area were undertaken along pre-planned and pre-selected traverses in order to investigate the geological setting and mode of occurrence of the Ikanga iron ore deposit.

2.2.1 Petrographical analysis of rock samples

Petrographical analysis of rock samples in thin section (Griffen and Phillips (2004)) was carried out under plane polarized light and under crossed nicols in order to identifty the mineralogical composition of the host rocks of the Ikanga iron deposit. The characterization of the mineralogic composition facilitated identification of the host rocks in the project area.

2.3 Ground Magnetic Method

Ground magnetic survey in mineral exploration is a geophysical technique that is applied to map subsurface formations. The basic principle is to determine magnetic ore minerals including various combinations of induced and remanent magnetization that perturb the earth field (Reynolds et al., 1990; Hanna, 1969; Criss and Champion, 1984). Measurements are made using fluxgate, proton-precession, overhauser, and optical absorption magnetometers.

2.4 Magnetic Surveys and Instrumentation

Magnetic surveys for minerals usually involve the use of a total field magnetometer. The magnetometer most commonly used is the proton precession magnetometer whose basic principles are briefly outlined below.

2.4.1 Proton precession magnetometer

The proton precession magnetomer which is designed to measure the total magnetic field of the earth. Its sensor comprises a cylindrical bottle filled with a liquid rich in protons (hydrogen atoms) (Figure 2.1 (a)). Each of these protons possesses a magnetic moment which acts as a small magnet. The magnetic moments align themselves in the direction of the earth's magnetic field, Be (Figure 2.1 (b)). On applying a stronger magnetic field (Bp) through a coil wound round the bottle, the protons are realigned in the resultant field (Figure 2.1 (c)). However, when Bp is switched off, the magnetic moments return to be aligned once again with the earth's magnetic field, Be. As this takes place, the magnetic moments precess at a characteristic frequency, ω, that is proportional to Be, expressed as

$$\omega = \gamma_p B_e,$$

where γ_p is an an accurately known constant known as the gyromagnetic ratio of the proton (Figure 2.1 (d)). The frequency ω is measured by a weak radio signal emitted by the precessing protons.

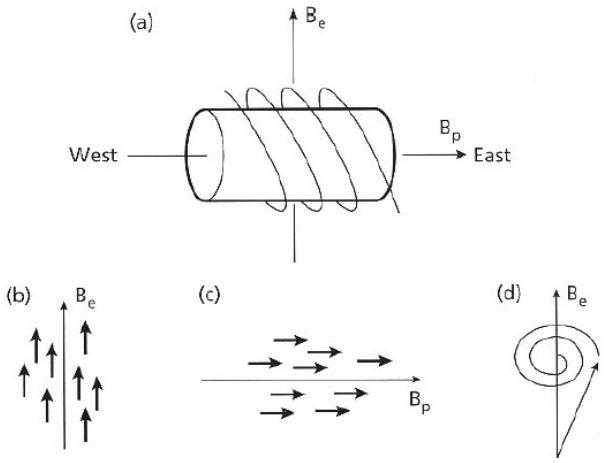

Figure 2.1 Principle of the proton precession magnetometer

The proton precession magnetometer measures the total magnetic field of the earth and, therefore, the alignment of the instrument is not required. Consequently, it is admirably suited to airborne and submarine measurements. Its disadvantage is that it measures the magnitude of the total ambient field and not its direction.

2.4.2 Data acquisition, processing and interpretation

Data acquisition, processing and interpretation involve the components of ground survey followed by data processing and interpretation. These components involve the following approaches.

2.4.2.1 Ground surveys

To carry out a ground survey, first, a survey grid is established by staking out a baseline parallel to the geological strike and traverse lines normal to the baseline. Measurements are taken on reading stations located along the traverse lines. A reference or base point is identified in the vicinity of the survey and readings are taken at this point at certain intervals during the survey, normally at intervals of 1-2 hours. It is mandatory that the day's survey must start off and close off with a reading at the base point. The base point is usually located in the area where the magnetic field has approximately the value of the undisturbed main field of the earth.

The distance between observation points depends on the type and purpose of the survey. For mineral exploration, the distance between the observation points is normally between 5-25 m. The observation points should be sufficiently far removed from disturbing objects such as railways, steel constructions, etc. A safe distance is 150 m. The observer should not carry with him/her any metallic articles such as penknives, watches, keys, etc.

2.4.2.2 Magnetic data acquistion method

Magnetic data were acquired in the field along fifteen (15) profiles at the end of every twenty-meter interval through the use of the proton precession magnetometer. A Brunton compass was also used to accurately direct and control the traverse directions perpendicular

to the established baseline on the established grid. For accuracy, GPS was used to mark magnetic data sampling localities and these positions were then recorded as UTM coordinates in a field note book. A total of 500 magnetic data samples were collected on this grid along these traverse lines.

2.4.2.3 Magnetic data correction

The IGRF correction is done by subtracting the average magnetic reading of every station from the regional field of the study area (33, 512.7nT). This correction is made to compensate for the anomalies/noises in the study area during at the time field measurements are made and magnetic data is collected.

2.4.2.4 Data processing and interpretation

The magnetic data are usually corrected for diurnal variations using simple interpolation and correction programs. The processed data are then subjected to any one or more of available automated interpretation software packages such as those involving 2-D or 3-D Euler deconvolution algorithms, among others. The Euler deconvolution algorithms make use of Euler's differential equation to invert the magnetic data to obtain the spatial locations of the magnetic sources in the earth's medium. In the 3-D case which was used in this research project, the Euler deconvolution program gives as output three parameters: the x-, y- and z-locations of the magnetic sources, where the z-location corresponds to depth-to-magnetic source from the sensor.

2.5 Geochemical Data Acquisition and Processing

Samples collection in the field for geochemical analysis was done by using a rock hammer for outcrops. The samples obtained weighing at least one kilogramme each were parceled at and sealed up and numbered. Similarly, soil samples were collected, sealed and numbered in the same manner. The both sets of samples, with standards and duplicate samples were transported to the laboratories of the Mines and Geological Department in the Ministry of Mining in Kenya for geochemical analyses using the atomic absorption spectrometric analytical method. Every sample point in the field was located using GPS and the UTM coordinates in the field notebook.

2.5.1 Atomic absorption spectrometric analysis

The technique makes use of absorption spectrometry to assess the concentration of an analyte in a sample (Walsh, 1955; L'Vov, 2005). It requires standards with known analyte content to establish the relation between the measured absorbance and the analyte concentration. To get the weight loss on ignition (LOI), samples were weighed first then heated under high temperature at 1000 C^{o} (degrees Celsius) in the furnace, cooled and then weighed again before further processing. LOI was then calculated. Results of the sample analyses were displayed electronically and the readings recorded.

2.6 Materials, Equipment, Data Sets and Software Used

The materials and equipment used in this study includes proton precession magnetometer, GPS, compass, geological hammer, camera, maps, satellite imageries, field note books, safety boots, sample bags, permanent markers, pencils and pens, and rock sacks.

2.6.1 Data sets used

Two sets of data (Primary data, and Secondary data) were used to conduct this study.

2.6.2 Primary data

The primary data of this study were acquired in the field and in the geochemical laboratory through mapping, data collection, and geochemical analyses of samples. The primary data include the magnetic data and geochemical data.

2.6.3 Secondary data

The secondary data include geological and topographical maps, and researched papers by other researchers on the study area and its surroundings.

2.6.4 Software used

3D Euler deconvolution, and Arc-Gis 10.0 were applied in this research. The 3D Euler deconvolution was used to analyze the magnetic data. The basic concept of the 3D Euler is to estimate the source location, depth and SI (structural index) simultaneously assuming

constant background (Hsu, 2002; Geroovska et al., 2005). This approach is fully automatic and yields reliable estimates if the background field can be adequately represented as a constant. Estimation is made for both the source location and SI using Euler deconvolution assuming nonlinear background. Arc-Gis 10.0 was also applied to create maps and digitize preexisting ones. The magnetic data acquired in this study are presented in the Appendix.

CHAPTER THREE: GEOLOGICAL SETTING OF THE IKANGA IRON DEPOSIT

The regional and local geological settings of this study area are discussed in this Chapter in which an attempt is also made to establish a correlation between the geology of the study area and the general geology of East Africa in summary.

3.1 Regional Geological Setting

The Neoproterozoic Mozambique Belt in Kenya, Tanzania and Uganda, represents by far the longest geological segment of crustal mobility of the African Continent (Warden and Horkel, 1984; Schlüter, 1997). During the orogenesis of this belt, rocks of the African continent that were in the radii of this orogenesis were affected by this process and accompanied its evolutional trend. The result of this tectonic evolutional trend, led to the distribution of associated rock types in Mozambique, Tanzania, Kenya, Uganda and Ethiopia which are the most affected countries in the Belt. The lithologies and tectonic features of this belt varied, and comprised of metamorphic, sedimentary, and volcanic suite, including rifting, sedimentary basins, hills/mountains, etc. The extension of the Mozambique Belt is reflected in these tectonic, lithologic and structural features which formed the largest portions in East Africa.

The study area is located in a fractional segment of this regional Belt. The geological setting of the study area reflects the tectonic processes through which the Mozambique Belt has been subjected to since its emplacement. Some of the areas, for example, have no outcrops. Some contained peneplains, and other areas are rifted, lifted and contain well exposed rock outcrops, domes, valleys and basins. These conditions are fairly regional and variable. Hence, the regional distribution of the Neoproterozoic Mozambique Belt rocks and tectonic features occur in common in Kenya, Tanzania and Uganda (see Figure 3.1 below). The detailed theories of the geological evolution of the Neoproterozoic Mozambique Belt in Kenya, Tanzania and Uganda in East Africa are outlined in Schlüter (1997).

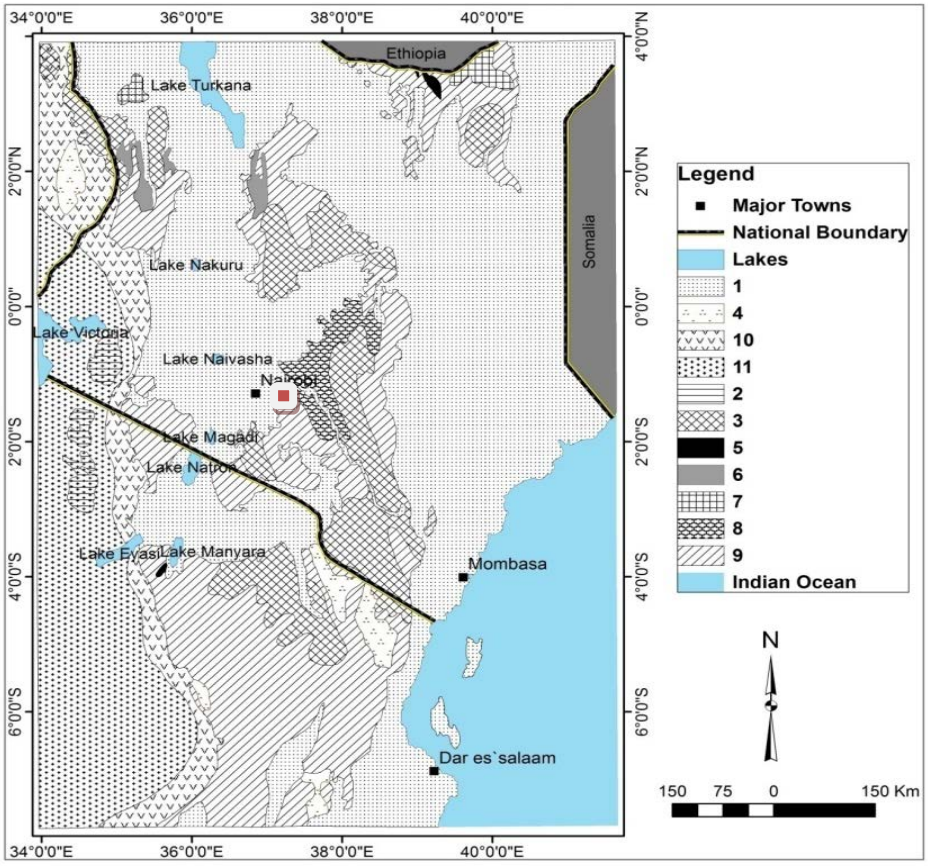

Figure 3.2 Distribution of rocks associated with the Mozambique Belt in Kenya, N.E. Uganda, and central and northern Tanzania with the study area showing in red dot. (Modified after Shackleton, 1986).

Explanation: 1=Phanerozoic cover; 2=Bukoban system and related formations; 3=Areas where marbles outcrop; 4=Predominantly granulite; 5=Ultramafics, probably ophiolites; 6=Mafic gneisses and schists, probably ophiolites; 7=Late Precambrian granites; 8= Tectonized granites; 9=Undifferentiated rocks of the Mozambique Belt; 10=Mylonitized Archaean rocks; and 11=Tanzanian (East African) Archaean Craton.

3.1.1 Bedrock geology

Bedrock in the study area consists of predominantly undifferentiated Neoproterozoic rocks consisting of gneissic complexes which are overlain by compacted Tertiary to Recent alluvial deposits. These rocks are considered as the dominant sources of much of the lithoclastic sedimentary sequences that are deposited in the study area. The bed rock geology of the South Kitui County where the study area is located was described in detail by Walsh (1959) and Schoemann (1948). The general strike of the rocks in the study area, is generally north-south and is in good accord with many of the other Neoproterozoic Mozambique Belt rocks so far mapped in Kenya (Walsh, 1959).

3.1.2 Pliocene-Recent sediments

Sediments in the area include alluvial deposits and volcanic ash. These deposits overlie the bed rock. They consist of poorly sorted sandy soils, coarser boulder scattered volcano-clastics and conglomerates on large scale erosional surfaces. These beds have been interpreted in other parts of Kenya as proximal alluvial fan deposits by Morley et al. (1992). Along the course of the north-south trending Nzeeu River occur alluvial deposits consisting mostly of fine sand with the occasional thin layers of grey silts which indicate seasonal flooding. The alluvial composition on the dried Nzeeu River beds consist of poorly sorted gravel-like pebbles derived from the rocks in the area and further afield.

3.1.3 Superficial deposits

Surface expression in the study area indicates red-brown soils, usually consisting of sandy deposits which are the weathering products of underlying bedrock. The dispersion of this surface pesolithic laterite is common. In areas of poor drainage, typical black cotton soils are developed which can be hard and fissured when dry and have the tenacity of clay when wet. Discontinuous layer of nodules of secondary kunkar limestones a few centimeters in diameter are localized below the surface. These secondary limestones are buff or pink in color due to iron staining and often include minor angular fragments of quartz and feldspars. The black soil depositional areas are always open grassland which have natural nutrients for vegetation growth.

3.2 Remote Sensing Results from the Study Area

The geological overall view of the study area was known prior to the start of the field work through the remote sensing application. Figure 3.2 below is a Landsat ETM+Band 3:1 ratio for iron oxide and displays the dispersion of iron oxides in the study area. This method also identified portions of the study area in which the concentrations of iron formation deposits are low and high, and shows parts of the area with bushes and sandy soils, low and high reliefs, drainage patterns, and, finally, the north-south trending Nzeeu River that cuts the study area into two parts as shown in Figure 3.2 below.

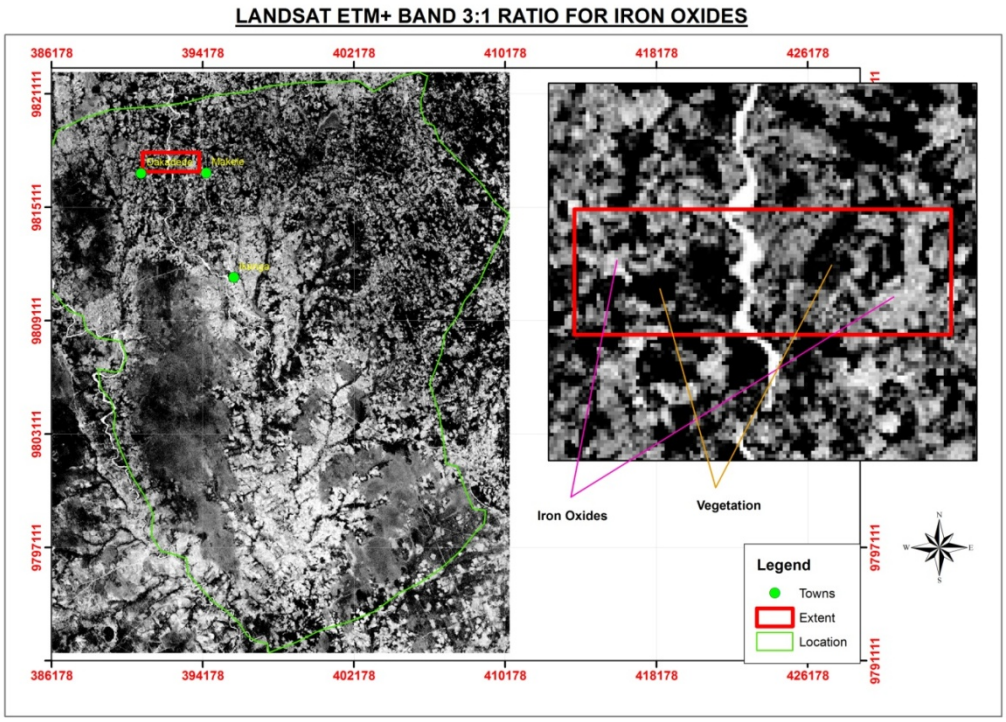

Figure 3.2 Satellite imagery of the study area showing iron oxides in light gray and dark color for vegetation (Source: Howell (2013), http/twitter.com/USGS Landsat images downloaded for free at: http/eros.USGS.gov/image gallery/or http//landsatlook.usgs.gov.).

3.3 Local Geological Setting

Geological samples and primary data representative of the geology of the study area shown in Figures 3.3 were collected. Figure 3.4 shows the geologic landscape. The landscape is jagged with sparse vegetation. The landscape reflects past tectonic activity and is also defined by faulting. From this partial view, a hill in the background and a flat area in the foreground are observable.. Critical samples related to the Ikanga iron deposit are shown in Figures 3.5 to 3.15 below. Gneisses are the dominant local rock types in the study area. Others include marble/limestone, sandy soils, alluvium, lateritic silica-baked-canga, and cutans deposits. The distinctive geological setting and physiographical features which are caused by tectonic rifting and block faulting, which affect sediment deposition and river drainage systems, match the surface and subsurface distribution of rock formations (Rop, 2011). The entire Ikanga area is best known for its Pliocene and Pleistocene strata, Cretaceous, Eocene, Oligocene, and Miocene which are derived from older rocks of the Archaean Age (Brown and McDouglas, 2011). Local outcrops mapped in the study area are presented in Figures 3.5 to 3.15 below. The local rock outcrop units in the study area **c**an be grouped into three.

The three groups are the gneisses, the lateritic ferruginous canga, and the marble/kunkar limestone. Each of these groups exhibits a different profile of weathering. The gneisses form unique widespread outcrops mostly along the Nzeeu River banks to the west. In the gneissic group, weathering produces chemical etching, and pulverization of the outcrops (see Figures 3.5 to 3.8 below).

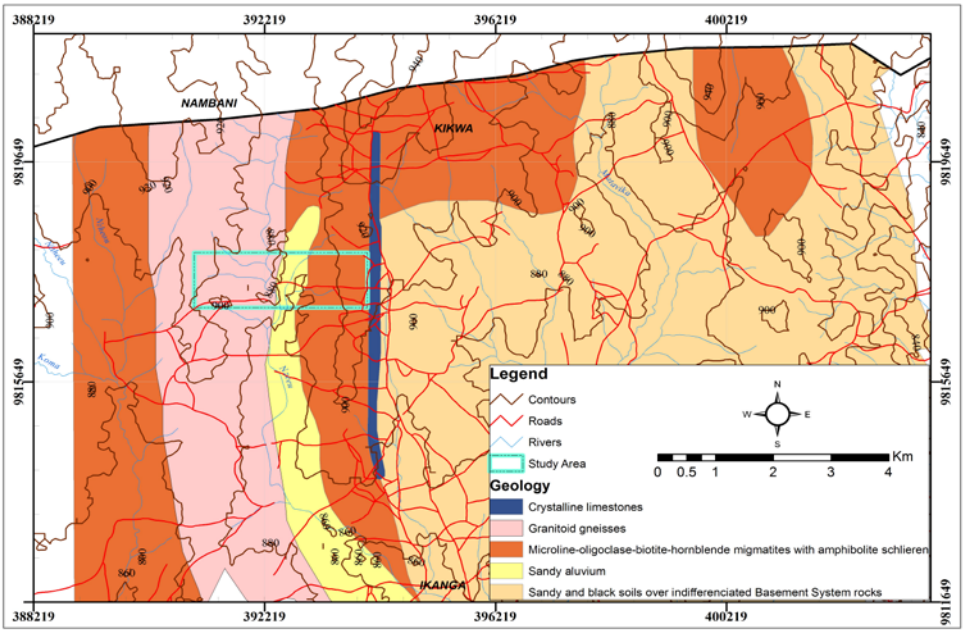

Figure 3.3 Geological map of the south Kitui showing the study area in the rectangle.

Figure 3.4 Widespread gneiss outcrops to the western front of the study area.

Figure 3.5 A Chemically etching gneissic outcrop that is showing interlocking crystals of brown, red, gray, and white colors with weak exfoliation fabric. The reddish brown-gray colours indicate the growth of iron oxide and the whitish colour exhibits the etching surfaces of the quartz that is set in the matrix of plagioclase feldspars).

Figure 3.6 Quartzo-feldspathic gneiss in which quartz veins are crosscutting each other at right angles.

Figure 3.7 A highly deformed quartz-feldspathic gneissic body showing multiple colours of iron oxide staining and some quartz fragments that are embedded in the deformed gneissic fabrics. Such deformational feature is common in the study area and is the function of prograde metamorphism and deformation.

Figure 3.8 A highly deformed gneissic body in which all primary fabrics have been destroyed.

Figure 3.9 Showing an outcrop of marble.

Figure 3.10 Figure 3.11

Figure 3.10 A well cemented lateritic caga deposit with hematite staining and silica baked contain iron. Canga is known for hosting iron which ranges approximately from 45%Fe to 60%Fe).

Figure 3.11 Lateritic ferrous-quartzite deposit with hematite coating in places on its surface areas. This lateritic ferrous quartzite surface deposit shows that there are some iron enriched bodies within the subsurface rock formations.

Figure 3.12 Cemented silica baked canga deposit.

Figure 3.13 A hematite/magnetite nodular deposit.

Figure 3.14 Remains of a brick kiln in the Ikanga area.

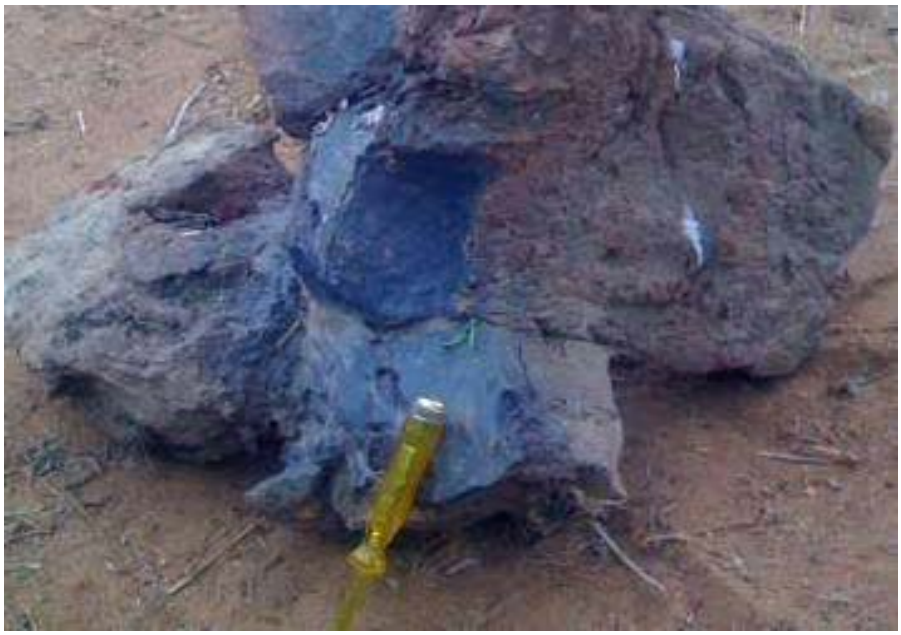

Figure 3.15 Showing heated bricks converted to a cemented iron rich brick mass. These hematitic temperature baked nodules are show that the soils contained a considerable iron content. This condition occurs in few places within the study area and its surroundings.

The granitoid gneisses are resistant to weathering and occur as stranded tors and hills in the study area (Figure 3.4). The weak gneissic fabric on the rock outcrops is distinctly enhanced by the surface weathering effects (Figure 3.5). The granitoid geneisses essentially consist of quartz, plagioclase, alkali feldspar and minor biotite. Presence of reddish brown grains of garnet dispersed in the rock indicate medium to high grade metamorphism. In other instances, blebs of quartz veins were noted to stretched out and folded in the quartzo-feldspathic gneissic rock (Figure 3.6). Fabric is a very useful textural feature in identification of fresh rock in fresh rock. Its value, however, is greatly diminished where the weathered rock has been largely pulverized by deformation and metamorphism. Where weathering has been intense like in the study area, kaolinite and Fe-oxides are commonly the end products of the weathering of mafic and felsic rocks(Figures 3.6 and 3.7). Quartz which occurs as anhedral strained grains is the only completely unaltered mineral. The whole area is mantled by red, friable sand-clay soil and strewn with multiple component materials with metamorphic cemented laterite outcrops protruding.

The second group of lithologic surface outcrops noted in the study area are the Fe-rich cemented ferrous laterite-canga (Dorr, 1964; Glossary of Geology, 1980) is the cemented metamorphic ferrous which this study seeks to investigate. Cementation in lateritic outcrops as shown in Figures 3.10 and 3.11 is one of the most recognizable features in laterite profile regime that occur in response to the change in modifications in laterite profile regime occurring in response to the change from a humid to an arid climate (Robertson, 1991). In such case, the most common cementing agents are iron oxides (ferricrete); silica (silicrete hardpan); calcium and magnesium carbonate (calcrete); aluminosilicates and gypsum. In summary, By definition, ferricrete is an indurated material formed by the in-situ cementation of pre-existing regolith by iron oxides. The fabric, mineralogy and composition of ferricretes reflect those of the parent material (regolith) and if residual, the underlying lithology. On the other hand, a silicrete, it is an indurated regolith component, commonly having a conchoidal fracture with vitreous lustre. Silicrete in the study area (Figure 3.12) is represented by near-complete complete or near-complete silification of an Fe-rich precursor regolith horizon by the infilling of available voids with silica. These iron bearing outcrops are common in the study area. Apart from the cemented lateritic iron caps within the study area, the occurrences of distinct iron mineralization in the form of haematite-magnetite nodules and fragments were also noted (Figure 3.13). The soils in the study area were noted to be enriched in iron content. A case in point where soils were noted to have higher contents of iron was at a locality along

R-iver Nzeui where a brick making activity was taking place (Figure 3.14). Due to the exceptionally high contents of iron in the soil, the majority of burned bricks in this kiln fused together to form composite metallic units as shown in Figure 3.15 instead of coming out as single brick units. As a result of this phenomenon, the owner of the brick making kiln incurred a loss on investment. This, however, may be a blessing in the long run in that it provides evidence for possible occurrence of iron mineralization in the study area. It is, therefore, interpreted in this study that the enriched Fe-content in the baked bricks resulted in the fused composite metallic bricks (Figure 3.15). The regolithic soil horizons in the study area are haematite rich, and if concentrated can form a reasonable mineable deposit. It is, however, important to note that for iron formation to become mineable it requires that it must be of reasonable thickness, width and length within the same locality.

The third major group of lithologic surface outcrops are the crystalline marble units (Figure 3.9) which texturally show some banding features and loose kunkar limestone in scattered areas within the study area.

3.4 Structure and Metamorphism

Like many other areas in Kenya, the sequence of events appears to have been firstly deposition of sediments, secondly widespread folding with accompanying regional metamorphism, and lastly granitization (Walsh, 1959, p.25). Rocks in the study area are folded into a synform with the axis trending N-W to S-E. The dominant foliation in these rocks is marked by the alignment of phyllosicates, hornblende, and pyroxene, and parallels the axis of the synform. Microtextures observed in thin section exhibited co-existence of strained and unstrained minerals. This suggests pre-, syn-, and post kinematic growth of metamorphic minerals resulting from multiple episodes of deformation in rocks (Boadi, 1991). In the study area there are less defined outcropped beds upon which to do accurate measurement of strike and dips on due to deformation and metamorphism of rocks. However, some strikes and dips were measured on available outcrops (see Figure 3.16 below). Little evidence of faulting was also recognized within the study area mainly because of complications in the stratigraphy and poor exposure. The style of deformation indicates that shearing and plastic flow was dominant over brittle failure and, therefore, such indicated faults may be post-metamorphic structures. The general strike trend in the study area also

corresponds to other structural trends mapped in other parts of Kenya within the Neoproterozoic Mozambique Mobile Belt (Walsh. 1959).

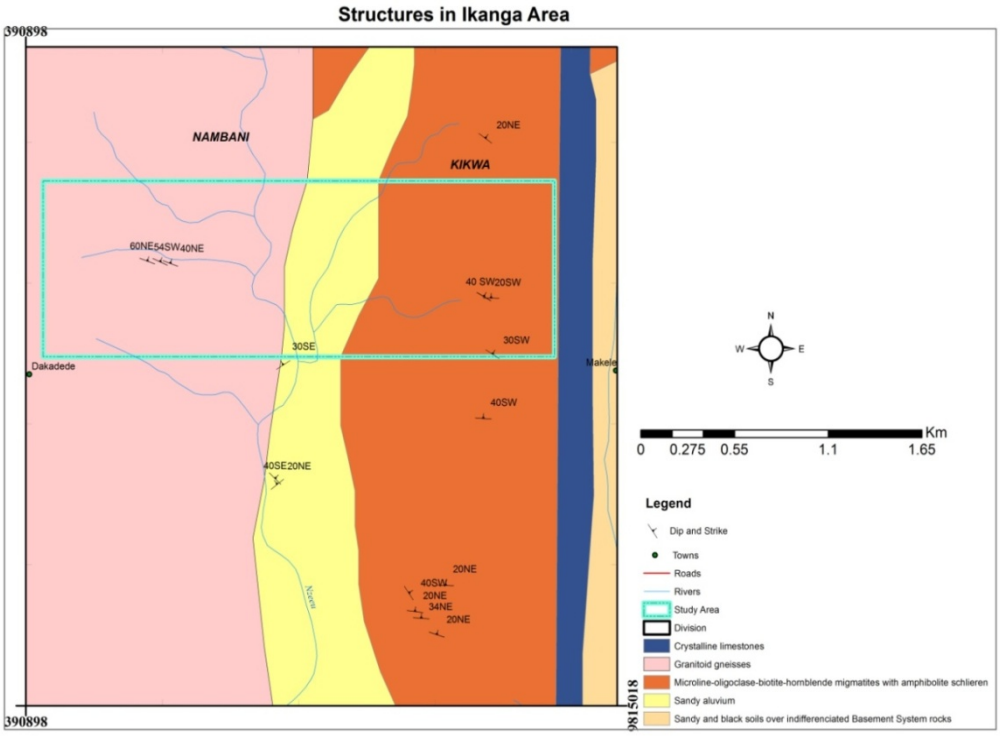

Crystalline Limestone

Granitoid gneiss

Microline-oligoclase-biotite-hornblende migmatites with amphibolite schlieren

Sandy alluvium

Sandy and Black soils over indifferenciated Basement System rocks

Figure 3.16 Showing the structural trends of rocks in the study area and its surroundings. Source: D.O.S 423(Series Y731), Edition I-D.O.S., Published by the Directorate of Oversea Surveys for the Kenya Government, Sheet 164/1, 1965. The schematic stratigraphical column of units forming the Local Geology of the study area is presented above.

3.5 Petrographical Thin Section Analyses

Thin sections analyses of these rocks from the mainly north-south trending collisional Neoproterozoic Mozambique Mobile Belt defined the temperature/pressure (T/P) metamorphic conditions which the rocks of the study area have been subjected to. The orientation of mineral cleavages in thin sections indicated the rearrangements of the rock fabric as being the results of internal, and external stresses reflecting the tectonic history of the high grade Ikanga area.

3.5.1 Biotite-hornblende schist

This is an intermediate medium grained metamorphic rock with a preferred schistose fabric. It consists essentially of plagioclase, biotite and amphibole.. Most of the plagioclase crystals show some minor alteration to sericite and can be recognized by the presence of multiple laths showing albite or lamellar twinning. Coloured minerals include biotite, pale green hornblende and minor greenish augite. Under plane polarized light (PPL), biotite is highly pleochroic from pale yellow to deep brown (Figure 3.17). Accessory minerals include quartz, magnetite, apatite and muscovite. The approximate mineralogical composition of a representative sample identified as biotite-hornblende schist is presented in Table 3.1.

3.5.2 Biotite-quartz-feldspar gneiss

The biotite-quartz-feldspar gneisses are widespread rocks in the study area. They are medium to coarse grained, mesocratic and well foliated with color banding or mineralogical layering of feldspar and opaque minerals. There is localized occurrence of garnet bearing gneisses particularly along the shear zones. Under the microscope the rock consists of plagioclase, orthoclase, microcline, quartz, biotite, garnet and accessory magnetite and muscovite (Figure 3.18). More than half of the feldspar in this rock is microcline feldspar. The cross-hatched twinning, characteristic of microcline, is visible. The quartz grains, which occupy the inter-granular spaces between the alkali feldspars, are easily recognized in Plane Polarized Light (PPL) by the lack of alteration, and in under Crossed Polars (XPL) by its interference colours which are slightly higher than that of the feldspars, and by the non-uniform extinction. Apatite, zircon and titanite (sphene) occur as accessory minerals. The mineralogical composition of a representative sample (GN-03) identified as a biotite-quartz feldspar gneiss, is presented in Table 3.1 above. Also noted to occur within this rock unit are amphibole bearing enclaves, which are possibly disrupted mafic dykes. These enclaves have biotite rich

margins, suggesting that small-scale mobility of alkalis and fluid phases took place during metamorphism and account for the formation of these hydroxyl-bearing minerals. The modal composition of this rock sample (LBD/ 13/GN-03) is presented in Table 3.1.

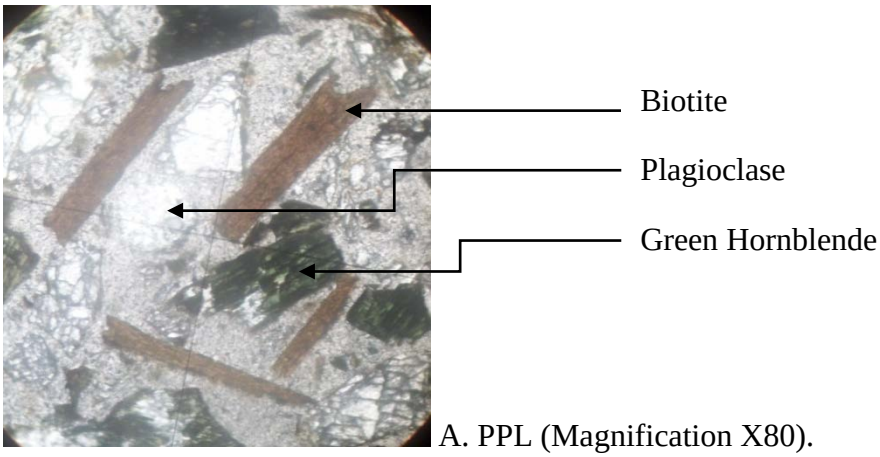

A. PPL (Magnification X80).

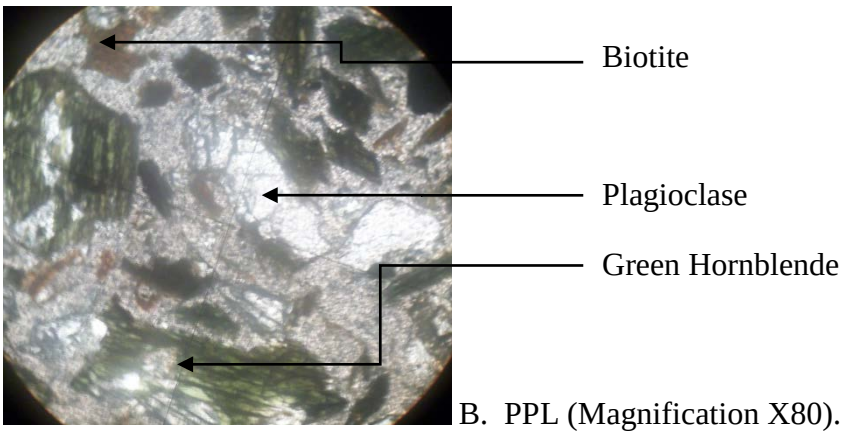

. B. PPL (Magnification X80).

Figure 3.17 Biotite-hornblende schist. (A). Note the tabular brown biotite grains B. (Magnification X80). B. Note the prismatic pale green hornblende with characteristic cleavage intersecting at 124^0/ 56^0. (Plane Polarized Light (PPL), Magnification X80).

Table 3.1 The modal mineralogical composition of rock samples from Ikanga area.

SAMPLE/ MINERAL	**GN-06**	**GN -03**	**PEG-01**
Quartz	5	33	29
Plagioclase	33	23	20
Alkali feldspar	10	29	42
Biotite	18	12	5
Muscovite	3	1	2
Hornblende	25	0 .5	0.5
Opaque	2	1	1
Accessories(Apatite, Zircon, Sphene	1	0.5	0.5
Total	**100**	**100**	**100**

NB:GN-06 – Biotite-Hornblende schist; GN-03 – Biotite –quartz feldspar gneiss; PEG-01-Pegmatite.

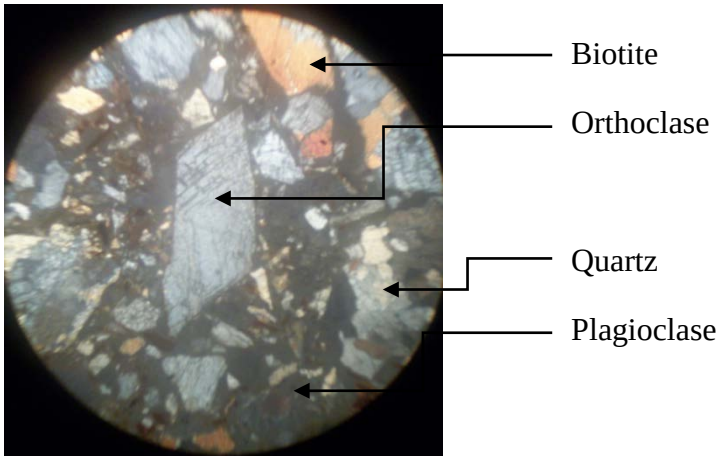

A. Crossed Polars (XPL)(Magnification X20).

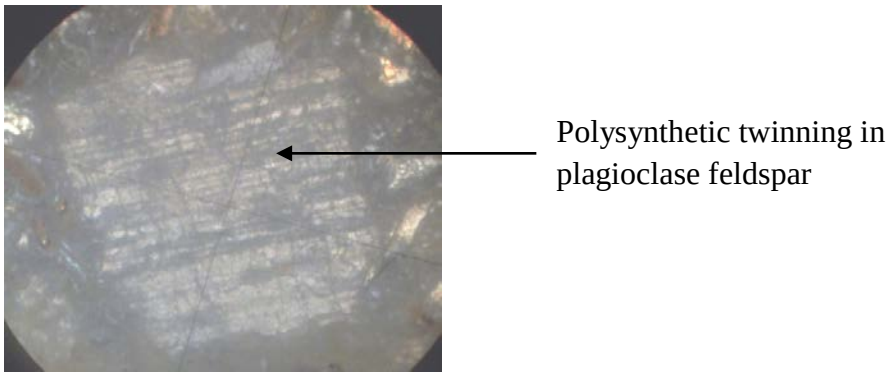

B. Crossed Polars (XPL) (Magnification X80).

Figure 3.18 Thin section micrographs of biotite-quartz-feldspar gneiss from the Ikanga area (Sample GN-03).

3.5.3 Pegmatite and quartz veins

Pegmatite is a very coarse grained rock that is interpreted to have been formed during the last phases of magmatism and/or metamorphism in this area. The pegmatites occurring in the Ikanga area are mostly pinkish in colour, and are composed mainly of alkali feldspars (orthoclase and microcline), sodic plagioclase and quartz. Under the microscope, the pinkish feldspar is identified as microcline (Figure 3.19). Apart from the scarce inclusions of biotite and quartz crystals, the rock consists essentially of an intimate intergrowth of potassium-rich feldspar and sodium rich feldspar. This perthitic texture is exemplified by the fairly broad sinuous lamellae of albite that forms a braided pattern in an orthoclase host. Other pegmatite bodies showed graphic texture and abundant mica flakes, and sometimes garnet granules. The graphic texture is interpreted to be as a result of simultaneous crystallization of quartz and feldspar. Quartz veins, which occur in many of the rock, were noted to be lensoidal in shape

or stigmatically folded. The veins are interpreted to be the last products of either felsic intrusions or are simply derived from existing quartzo-feldspathic country rocks during metamorphic differentiation.

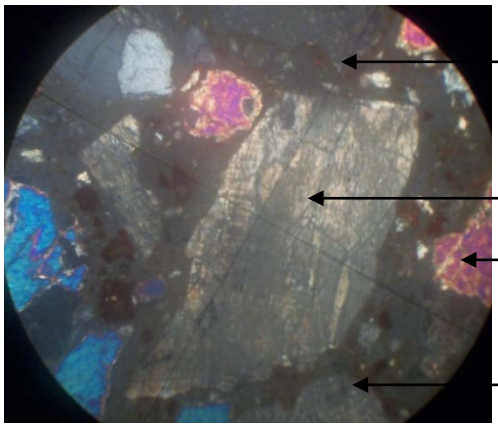

A. Crossed Polars (XPL)(Magnification X20).

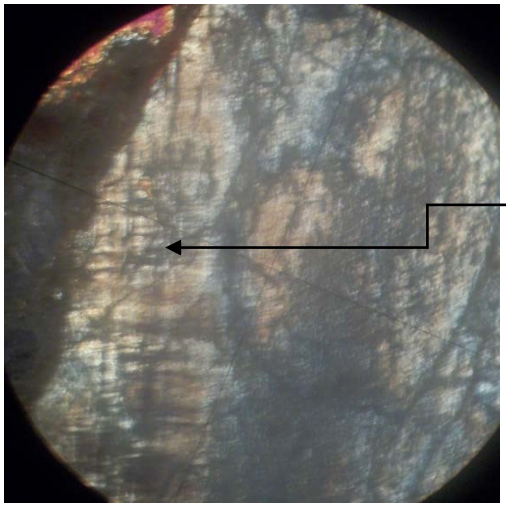

B. Crossed Polars (XPL)(Magnification X80).

Figure 3.19 Thin section micrograph of pegmatite showing (A) microcline, biotite, quartz and muscovite. (B) the characteristic cross-hatched twinning in microcline feldspar.

3.5.4 Biotite gneiss

Thin section of biotite gneiss analysed consisted of phlogopite, biotite, quartz, amphibole, and plagioclase. In thin section, biotite is typically brown, brownish green or reddish brown, and distinctly pleochroic. Intensity of colour increases with increasing iron (Fe) content. Phlogopite is nearly colourless to pale brown in thin section and has less intense colours than biotite because of lack of iron content. Quartz is colourless in thin section and twinning is not observed in thin section because the twin segments have the same ***c*** axis orientation.

Amphibole is distinctly coloured and pleochroic, usually in shades of green, yellow-green, blue green, and brown. Plagioclase has low relief, lack of colour, has biaxial character, and exhibits polysynthetic twinning which distinguishes it from other minerals. It is colourless in thin section (Figure 3.20).

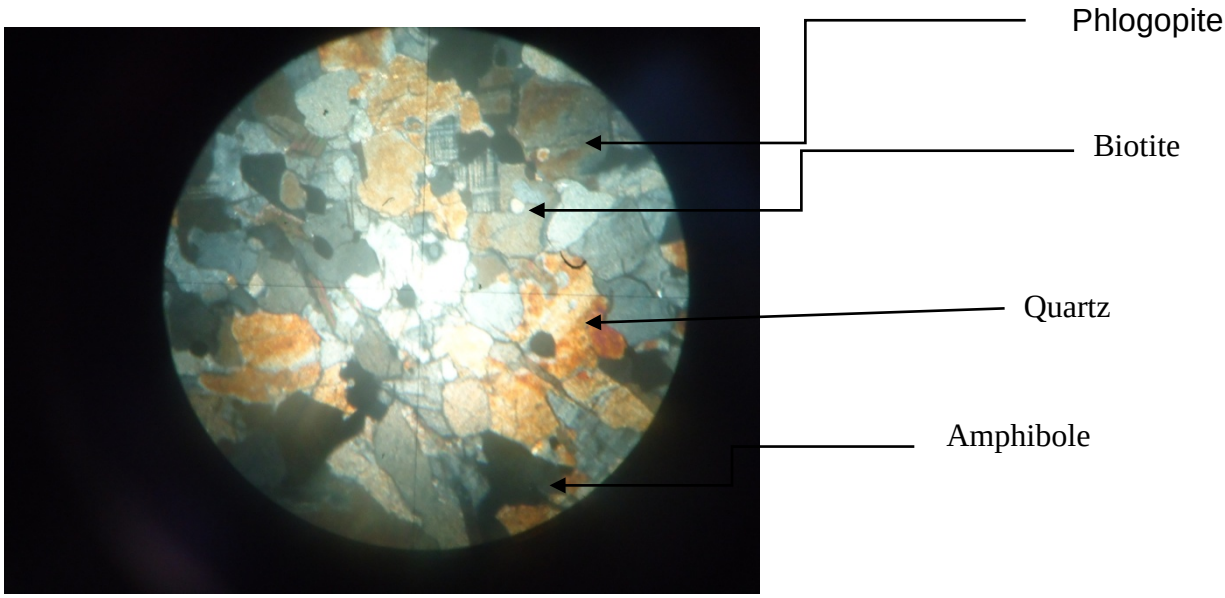

Figure 3.20 Thin section micrograph of biotite gneiss showing biotite, amphibole, quartz, and phlogopite.

CHAPTER FOUR: RESULTS OF THE GROUND MAGNETIC SURVEY AND GEOCHEMICAL DATA ANALYSIS

This chapter presents the results of the ground magnetic survey and the geochemical data analysis of the Ikanga area in Kitui, southeastern Kenya.

4.1 Magnetic Data Acquisition

Acquisition of magnetic data was achieved along fifteen (15) traverses at the end of every twenty (20) meter interval in the study area as shown in Figure 4.1 below.

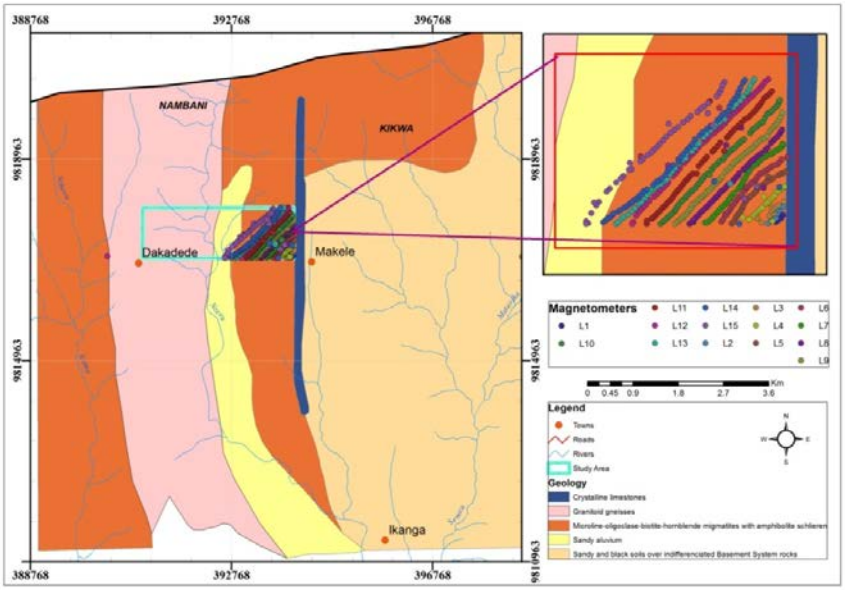

Figure 4.1 Showing profiles along which the magnetic data were collected.

4.2 Field Surveys and Results

The survey involved the use the MP II Proton Precession Magnetometer from Syntrex Ltd of Toronto, Canada. The data were corrected for diurnal variations and then sujected to a 3-D Euler deconvolution process using Oasis Montaj software from Geosoft Inc. of Canada. Figure 4.2 shows the resulting total magnetic field image (TMI). The total magnetic image in Figure 4.2 indicates a major magnetic high centred on the south eastern side of the area. From here, it spreads outwards in following a southwest and northeast trend but with a lesser magnitude. Another magnetic high appears on the southwestern side of the area trending nearly north-south. A major magnetic low that trends northeast to north occurs in the near

cetral part of the area. It appears to occupy a shear zone that trends generally southwest-northeast.

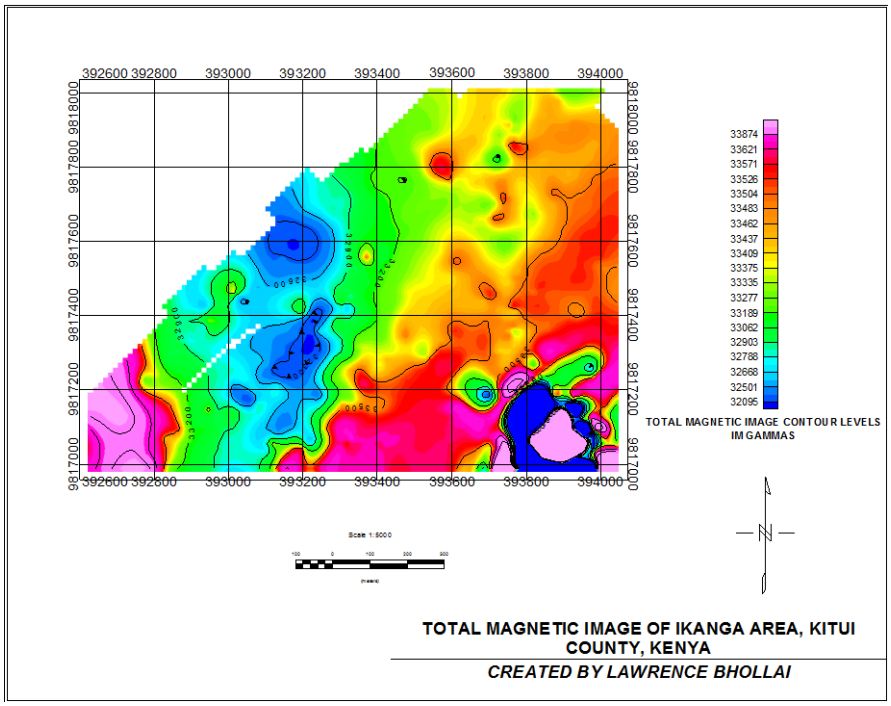

Figure 4.2 Total magnetic image (TMI) of Ikanga area.

Figure 4.3 shows the same total magnetic field image given in Figure 4.2 but with magnetic source depth location symbols superimposed on it. The depth symbols simply mark the lateral location of the magnetic source and the value of depth at which it occurs underneath the ground surface. The symbols and the corresponding values they represent are shown as a legend below the map. From the map, the magnetic source symbols are seen to follow a general southwest-northeast direction. They occur at a general boundary between the main magnetic high to the east and the main magnetic low to the west.

4.3 Discussion of the Results from the Magnetic Survey

From the two figures, magnetic source symbols mark the locations and orientations of linear structures at depth caused by shearing and subsequent mineral alterations. The areas occupied

by the magnetic highs may coincide with the locations of the iron formations. Ground truth investigations should be conducted to verify this assumption.

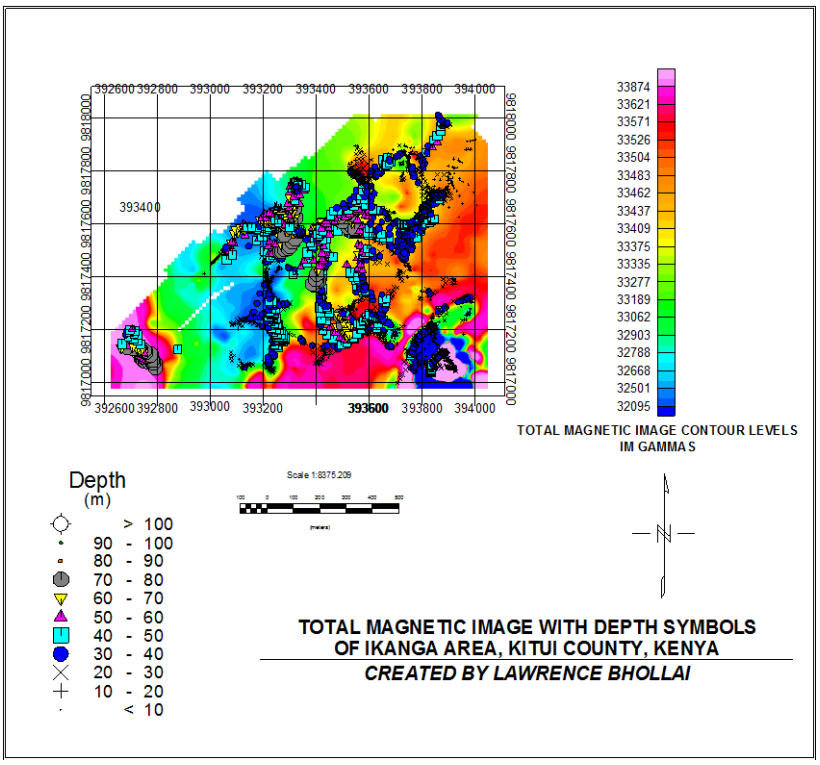

Figure 4.3 Total magnetic image (TMI) of Ikanga area with depth symbols.

4.4 Geochemical Data Analyses

The geochemical sampling localities superimposed on the generalized geological map of the area are shown in Figure 4.4. Further, these sampling localities referenced to the UTM Coordinate system are shown in Tables 4.1 below. A total of twenty four (24) samples representing the main lithological units in the project study area were collected for geochemical analyses. The characteristic lithological units sampled in this study ranged from ferruginous hematite, limestone, gneisses, soil to pegmatite and quartzite units. Geochemical analyses for this study were done at the Mines and Geological Department of the Ministry of Mining using the atomic absorption spectrometric (AAS) method. Analyses of the geochemical data from the study area showed predominantly oxide facies mineralization in

which Fe_2O_3 is the main iron oxide (see Tables 4.2 and 4.3 below) with low range percentage composition figures varying ranging from 0.05% Fe to 16.5% Fe, and the high range composition figures ranging from 72.4% Fe to 86.3% Fe in few places.

Table 4.1 Locality data for geochemical samples collected from the Ikanga project area referenced to the UTM Coordinate Map System.

Sample Ref. No.	**X UTM**	**Y UTM**	**Elevation (m)**
HEM-01	393648	9817335	917m
HEM-02	393554	9818273	918m
HEM-03	393466	9815390	910m
HEM-04	393975	9817226	913m
Lim-01	391713	9817542	892m
Lim-02	392451	9816332	892m
Lim-03	393359	9815845	900m
Lim-04	393006	9816420	903m
Lim-05	393989	9817240	902m
GN-01	393617	9817147	921m
GN-02	393520	9817517	910m
GN-03	393548	9817536	917m
GN-04	393362	9817904	908m
GN-05	393835	9817349	902m
GN-06	393617	9817147	921m
GN-07	393520	9817517	910m
S0-01	393006	9816420	903m
S0-01	393105	9817048	875m
SO-02	393119	9817060	784m
SO-03	393133	9817076	892m
SO-04	393105	9817048	782m
SO-05	393105	9817048	875m
PEG-01	393800	9817060	920m
PEG-02	393648	9817000	918m
QT-02	393737	9817148	901m

Key:
HEM=Hematite
Lim=Limestone
GN=Gneiss
SO=Soil
PEG=Pegmatite
QT=Quartzite

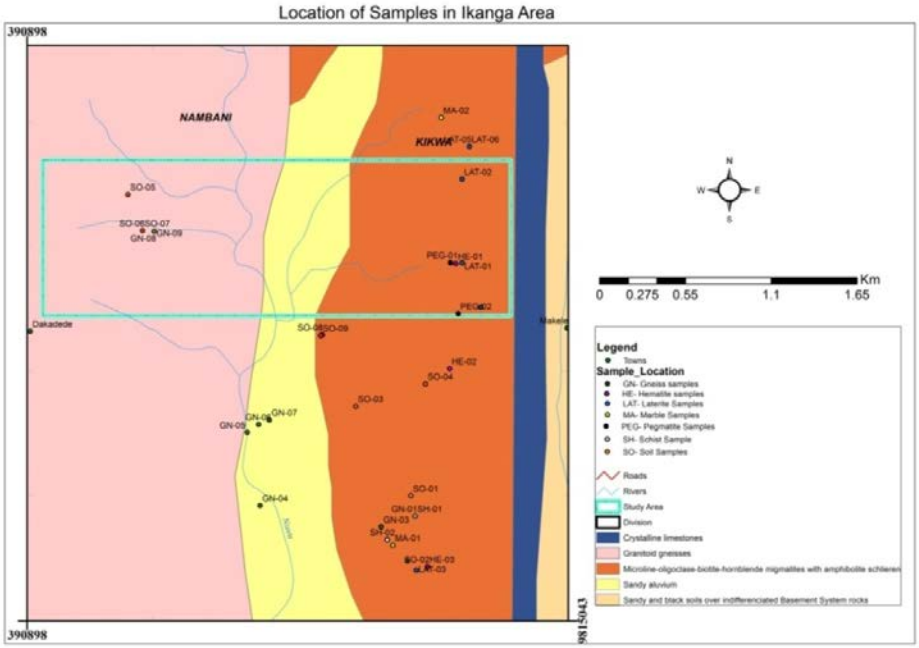

Figure 4.4 Geochemical sampling localities superimposed on the generalized geological map of the study area.

Table 4.2 Chemical composition of first set of rock and soil samples from Ikanga project - area. Major elements in weight %.)

1Sample#	SiO_2	Al_2O_3	CaO	MgO	Na_2O	K_2O	TiO_2	MnO	Fe_2O_3	LOI
Lim-01	1.92	0.09	54.7	0.42	0.04	0.07	ND	0.03	0.26	41.3
Lim-02	14.53	0.35	47.8	0.8	0.06	0.04	ND	0.1	1.95	34
Lim-03	8.64	ND	46.9	5.94	0.02	0.01	ND	ND	0.21	37.5
GN-01	44.97	8.07	23.7	1.22	0.52	1.76	0.35	0.06	4.03	14.2
GN-03	47	8.04	22.8	0.97	0.58	0.28	0.33	0.07	3.83	15.1
GN-04	51.78	8.97	20.6	0.96	0.66	0.1	0.27	0.04	3.38	12.4
QT-02	82.2	4.68	0.28	0.19	0.86	0.8	0.45	ND	5.79	1.47
S0-01	59.4	9.55	0.28	0.25	0.1	1.8	0.44	0.12	19	8.39

NB: Key: LIM = limestone, QT = Quartzite; GN = Gneiss, SO = soil; ND = not detected.

Table 4.3 Chemical composition of rock and soil samples from the Ikanga project area. Analysis done by using the atomic spectrometric method (AAS). Major elements in weight percent (wt%).

Sample #	**SiO_2**	**Al_2O_3**	**CaO**	**MgO**	**Na_2O**	**K_2O**	**TiO_2**	**MnO**	**Fe_2O_3**	**LOI**
HEM-01	9.79	0.44	0.08	0.34	0.16	0.06	1.11	0.2	86.3	Nil
HEM-02	20.59	0.44	0.66	0.32	0.14	0.04	4.7	0.2	72.4	Nil
HEM-03	10.07	3.4	4.91	0.54	0.3	0.04	2.02	0.2	76.3	Nil
HEM-04	23.67	0.42	0.1	0.31	0.2	0.07	0.89	0.14	72.9	0.57
Lim-01	1.92	0.09	54.7	0.42	0.04	0.07	ND	0.03	0.26	41.3
Lim-02	14.53	0.35	47.8	0.8	0.06	0.04	ND	0.1	1.95	34
Lim-03	8.64	ND	46.9	5.94	0.02	0.01	ND	ND	0.21	37.5
LIm-04	4.58	ND	34.4	18.7	0.14	0.02	0.02	0.01	0.05	41.3
LIm-05	1.17	ND	52.2	0.73	0.15	0.16	ND	0.1	0.47	43.1
GN-01	44.97	8.07	23.7	1.22	0.52	1.76	0.35	0.06	4.03	14.2
GN-02	68.16	6.58	0.16	0.36	0.25	0.79	0.5	0.2	16.5	5.91
GN-03	47.23	8.04	22.8	0.97	0.58	0.28	0.33	0.07	3.83	15.1
GN-04	51.78	8.97	20.6	0.96	0.66	0.11	0.27	0.04	3.38	12.4
GN-05	53.82	16.42	5.22	3.74	4.31	1.69	1.29	0.15	10.14	2.22
GN-06	68.81	12.97	2.8	1.07	4.09	3	0.69	0.02	4.35	1.25
GN-07	53.68	12.06	5.95	5.14	3.39	1.1	1.65	0.2	14.1	2.16
S0-01	59.4	9.55	0.28	0.25	0.1	1.8	0.44	0.12	19	8.39
SO-02	7.37	1.67	0.25	0.38	0.38	0.3	9.72	0.2	79.6	Nil
SO-03	61.9	21.8	0.09	0.14	0.19	1.4	0.74	ND	3.89	8.69
SO-04	64.55	18.64	1.57	1.17	2.27	3.6	1.22	0.06	5.8	Nil
SO-05	64.27	13.9	2.19	0.91	2.95	3.3	1.1	0.09	4.96	6.13
PEG-01	83.63	4.27	0.84	0.32	1.56	0.34	0.46	0.01	6.5	0.57
PEG-02	82.43	8.78	1.76	0.44	3.04	0.79	0.17	0.01	1.03	0.88
QT-02	82.2	4.68	0.28	0.19	0.86	0.8	0.45	ND	5.79	1.47

Key: LIM=limestone, QT=quartz, GN=gneiss, SO=soil, HEM=hematite, PEG=pegmatite, ND=not detected.

The Fe_2O_3 content in the haematite mineralized samples ranges from 72.4 to 86.3 wt% with an average of 76.97 wt%; 3.38 to 16.5 wt% with an average of 8.05 wt% in gneisses; and 3.89 to 79.6 wt% with an average of 22.65 wt% in soils. The geochemical setting of the Ikanga iron deposit in the study area suggests that it is derived from a Precambrian banded iron formation (BIF). When the Ikanga iron deposit data is plotted on diagrams to

discriminate global compositional fields of Precambrian BIF and Phanerozoic ironstones (after Patwardhan, 1999), samples from the Ikanga deposit show close geochemical affinity with Precambrian BIF (see from Figures 4.5 and 4.6). Correlation of the Ikanga iron deposit to the Precambrian BIF shows that the Ikanga iron deposit is derived from the Precambrian BIF by chemical weathering. The plot of geochemical data from samples of the Ikanga iron deposit on the global compositional field of the Precambrian BIF, confirmed this relationship (Figures 4.5 to 4.8 below). The plots further confirmed that the Ikanga iron deposit is not derived from Phanerozoic iron stones.

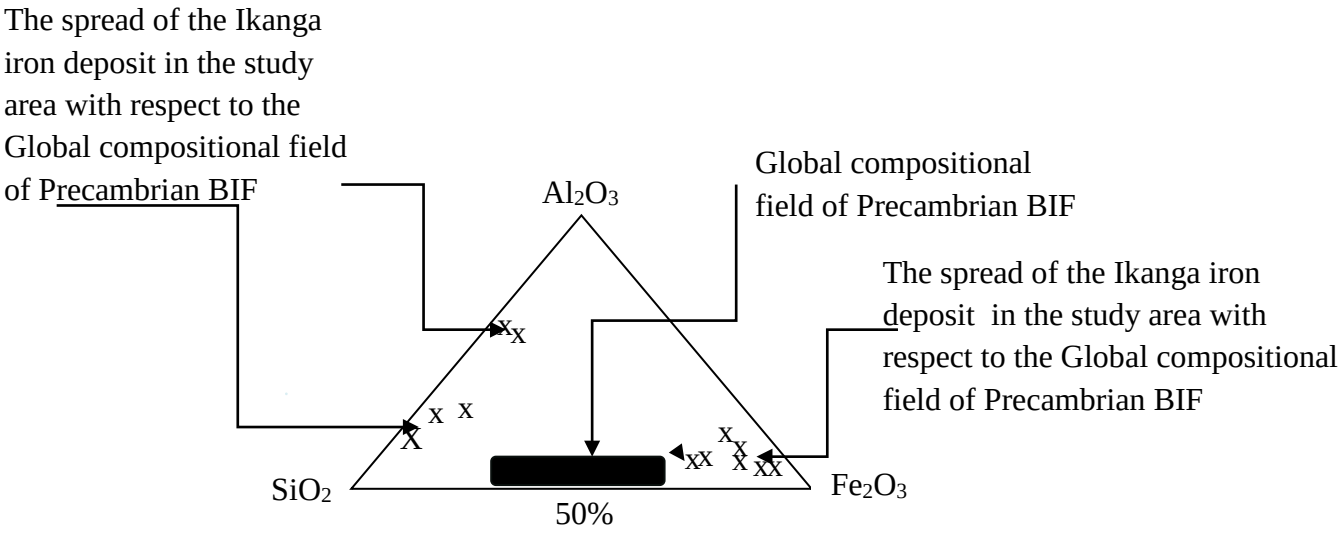

Figure 4.5 Global compositional field of Precambrian BIF, after Patwardhan (1999).

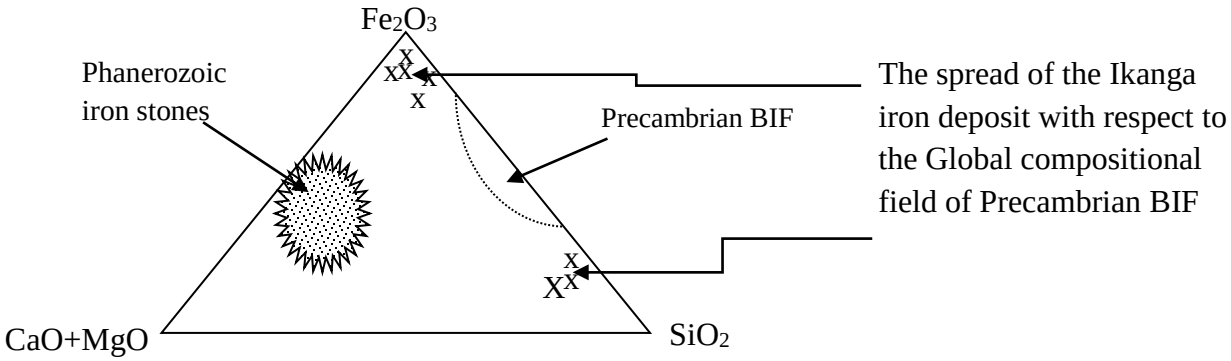

Figure 4.6 Compositional fields of Precambrian BIF and the Phanerozoic iron stones, after Patwardhan (1999).

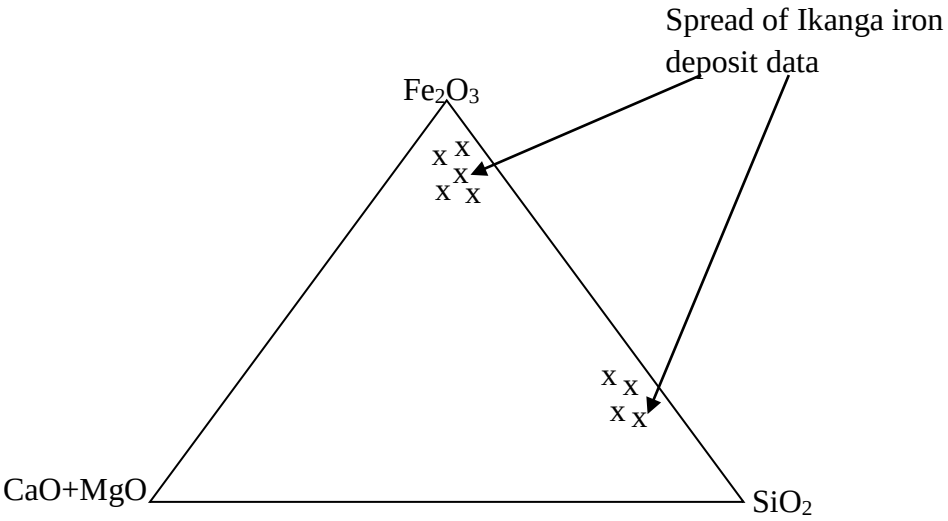

Figure 0.7 Showing compositional spread of Ikanga iron deposit on the scale of CaO+MgO, SiO_2, and Fe_2O_3.

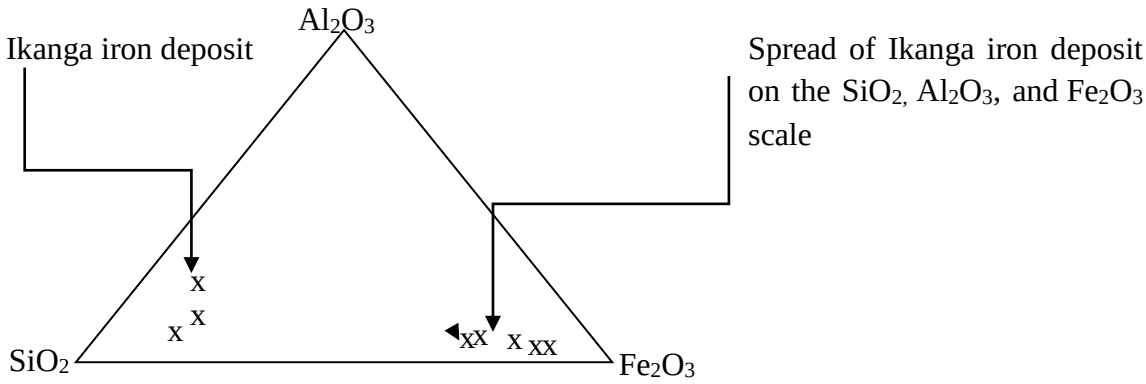

Figure 0.8 Compositional spread of Ikanga iron deposit on the global Precambrian BIF scale of SiO_2, Al_2O_3, and Fe_2O_3.

The compositional spread of sample data from the Ikanga iron deposit along the Precambrian BIF domain on the Fe_2O_3-SiO_2 side of the ternary diagram in Figures 4.6 and 4.7 confirms that the deposit was not derived from the more recent Phanerozoic iron stones. The geologic setting of the Ikanga deposit within the Neoproterozoic Mozambique Belt terrane further supports the geochemical evidence deduced from this study. Analyses of the geochemical data from the study area showed predominantly oxide facies mineralization in which Fe_2O_3 is the main iron oxide with percentage composition shown for all samples analysed (see Table

4.3 above). The geological data acquired from the study area indicated predominantly oxide facies mineralization in which Fe_2O_3 is the main iron oxide with the percentage analytical composition varying from a low range of 0.05 to 16.5 Fe_2O_3 wt% to a high range of 72.4 to 86.3 Fe_2O_3 wt% in few places.

CHAPTER FIVE: DISCUSSIONS, CONCLUSION AND RECOMMENDATION

In this Chapter, the results of this study are synthesized and discussed. Conclusions and recommendations are also presented.

5.1 Petrographical Thin Sections Analyses

Thin sections analyses of these rocks from the mainly north-south trending collisional Neoproterozoic Mozambique Mobile Belt defined the temperature/pressure (T/P) metamorphic conditions which the rocks of the study area have been subjected to. The orientation of mineral cleavages in thin section sections indicated the rearrangements of the fabrics of rocks as being the results of internal and external stresses reflecting the tectonic history of the high grade Ikanga area.

5.2 Ferrous Bearing Outcrops

Iron cap outcrop deposits commonly known as cangas are common in places to the highland portion of the study area mainly in the surroundings of the intersection of the north-south (NS) and east-west (EW) trending. Canga can be defined as a tough, well-consolidated rock consisting essentially of hard blocks and fragments of the rocks of an iron formation, cemented with limonite. Canga forms a valuable ore, which may run as high as 68% iron (Dorr, 2008; Glossary of Geology, 1980). Further, Anand and Butt (1988) and Anand et al. (1993) have provided the terminology and classification of deeply weathered regolith and addressed the issue of geochemical exploration in the complex lateritic environment of the Yilgarn Craton of Western Australia. Besides the metamorphic laterite enriched outcrops in the study area, the general soil also contains iron dispersion in its horizons. Less iron was reported in gneises, limestone/marbles, and quartz based on geochemical data analyses.

5.3 Mode of Occurrence of the Ikanga Iron Deposit

In considering the mode of occurrence of the iron deposit in the study area, it is necessary

first of all to define what iron formation are and how many categories these are divided into. The term iron formation was defined by James (1954), modified by Morris (1993) and reaffirmed by Klein (2002) in relation to banded iron formation as:

"A chemical sediment, typically thin bedded or laminated, whose principal chemical characteristic is an anomalously high content of iron, commonly but not necessarily containing layers of chert".

An original minimum iron content of 15 wt% (James, 1954) is loosely adopted by some researchers today (Ohmoto and Felder, 1987).

In terms of categories, the Archaean-Proterozoic banded iron formations (BIFs) are divided into three main categories. These are termed the Algoma; Lake-Superior and Rapitan-types and range in age from Archaean through to Paleoproterozoic to Neoproterozoic respectively (Gross, 1965; Gross, 1983). The Algoma-type BIFs were deposited during the Archaean (between approximately 3.5 to 2.6 Ga) and exhibit a volcanic arc-greenstone belt association (Gross, 1983). The Algoma-type BIFs are relatively thin (< 100m thick) and of limited areal extent (<100km^2), and have high iron oxide and silica contents. They are thought to be deposited in association with proximal oceanic hydrothermal plumes (black smokers). In terms of size, the Superior-type BIFs dominate the three BIFs categories. The largest examples of these BIFs have been calculated to contain > 10^{14} Mt of iron (James and Trendell, 1982), with examples on each of the five main continents (Simonson, 1985; Smith et al., 2000). These thick (>100m thick), and laterally extensive (>1000km^2) BIFs were deposited during the Paleoproterozoic (approximately 2.2 to 1.8 Ga) and represent the major period of iron deposition in the Earth's history.

The Superior-type BIFs generally consist of fine-grained iron oxides, carbonates or sulphides, and occur in planar form in mm- to cm- scale bands, usually alternating with similar scale bands of chert. The Rapitan-type BIFs are generally thin, usually restricted, and chert-poor bodies. Most are of Neoproterozoic age (approximately 0.8 to 0.6 Ga) and are thought to be the result of iron precipitation caused by oxidation after the retreat ice-sheets from previously covered, anoxic water bodies. The major global distribution of selected banded formations is presented in Figure 5.1 below. The mode of iron formation occurrence has been disputed. Both continental (e.g. Albert and McCulloch, 1993) and hydrothermal (e.g. Holland, 1973;

Simonson, 1985; Dymek and Klein, 1988) settings have been put forward as likely Fe-sources. In terms of source, older sedimentary iron bearing formations could be a source of iron. The Ikanga iron deposit which is the focus of this study may very likely have occurred as the result of the chemical weathering of older Precambrian banded iron formations (BIFs). If this is the case, therefore, it is a secondary deposit in which all of the banding and primary fabrics have been destroyed due to intense metamorphism and deformation over a prolonged geological period.

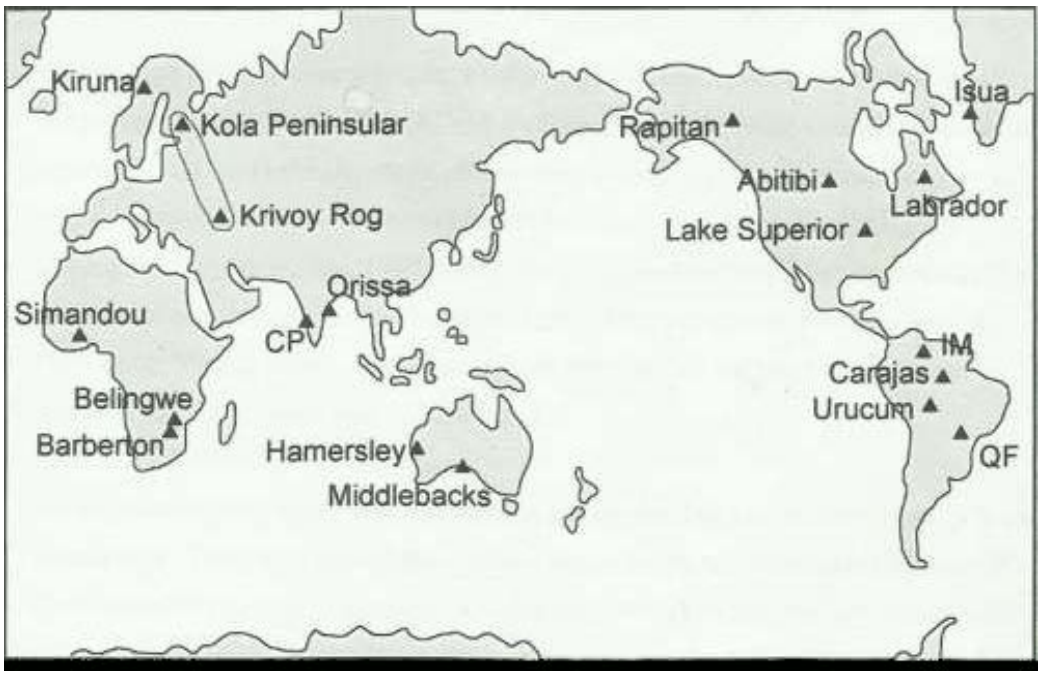

Figure 5.1 Global distribution of major and selected banded iron-formations and districts, modified after Klien (2002).

With such a prolonged geological history of the reworking of the Ikanga iron deposit, it became more granular and thinner and was dispersed in the regolith where it was localized within the upper most horizon in coexistence with other associated minerals. Its mode of occurrence can also be related to the Neoproterozoic iron bearing sedimentary deposits as reworked materials of Precambrian origin and may be described as marine iron bearing sedimentary deposit in this landmass. However, debate supporting the Archaean-Paleoproterozoic setting of iron formations cannot be ignored in this study. Ohmoto and Felder (1987) argued that Archaean-Paleoproterozoic iron formations are the precursors for secondary iron formations of which the Ikanga iron deposit is an example.

5.4 Discussion of Magnetic Data and Analysis of the Magnetic Signal Source Depth

Consideration of Figure 4.2 and Figure 4.3 indicates that the magnetic source symbols mark the locations and orientations of linear structures at depth caused by shearing and subsequent mineral alterations. The areas occupied by the magnetic highs may coincide with the locations of iron formations. Ground truth investigations should be conducted to verify this assumption. The reflections of magnetic analytical signals approximated the various depths from zero (0) meters on the surface to over one hundred (100) meters in the subsurface in which the Ikanga-type iron formation occurs. The variability of these depths indicates that the Ikanga iron deposit is scattered within the regolith. The movement of this iron formation is influenced by rain waters that seep downwards into the subsurface.

However, near surface secondary iron formation may also occur directly due to the conduction of high temperature heat (Hamade el al, 2003), or at lower temperature in the presence of water. For this reason dehydrated zones may repeat lower down in the hydrated and mottle zone and below where water may gain selective access through faulting and permeability to carry and deposit iron and associated minerals. Hence, Similar processes have been recognized in several ore bodies in the Hamersley Province of western Australia (e.g., Paraburdoo 4 East), where the upper most dehydrated layer is 10 m thick and, successively, lower levels become thinner (Clout, 2003).

5.5 Geochemical Data from the Ikanga Iron Deposit

The geochemical data analyzed from the project area indicated predominantly oxide facies mineralization. In this oxide facies domain, the Fe_2O_3 wt% is the main iron oxide. The Fe_2O_3 wt % in the hematite mineral analyzed rangers from 72.4 to 86.3 wt % with an average of 79.98 wt %; in gneisses the Fe_2O_3 content ranges from 3.38 to 16.5 wt % with an average of 7.97 wt%; and in soils the Fe_2O_3 content ranges from 3.89 to 79.6 wt % with an average of 22.65 wt %. These analytical results exceed an original minimum exploitable iron content described by James (1954).

5.6 Conclusions

This project was carried out within the stipulated time. The full understanding of the project area was accomplished through the field mapping work, field observations and data collection, and in the applications of remote sensing, geophysical and geochemical methods, and usage of approaches, materials, and software given in Chapter 2 of this dissertation. The conclusions were deduced from this research project-:

1. Rocks of the project area are Neoproterozoic in age commonly known as remobilized rocks of Precambrian origin. These rocks have been subjected to strain and stress associated with the high grade metamorphism of the north-south trending Neoproterozoic Mozambique Mobile Belt.
2. It is concluded that the study area corresponds to a particular geologic environment in the Neoproterozoic Mozambique Belt of Kenya, characterized by end of Neogene/Tertiary surface of gently and undulating elevations showing reworked Neoproterozoic rocks of Precambrian in origin with various litho-clastic sediments containing dominant oxide facies mineralization., Fe_2O_3 is the main iron oxide among the non-iron oxide domain of SiO_2, CaO, TiO_2, MgO, K_2O, MnO, Al_2O_3, Na_2O and SiO_2.
3. The analysis of the total magnetic image (TMI) of the area indicates a major magnetic high centred on the south eastern side and spreading outwards with lesser magnitude along a southwest-northeast trend. A major magnetic low trending northeast to north in the central part of the study area appears to occupy a southwest-northeast trending shear zone.
4. The analysis of the total magnetic image (TMI) of the study area and associated magnetic source symbols indicate that the depth symbols follow a general southwest-northeast direction and occur at a general boundary between the main magnetic high to the east and the main magnetic low to the west.
5. The magnetic source data mark the locations and orientations of the southwest-northeast trending linear structures at depth caused by shearing and subsequent mineral alterations. The areas occupied by the magnetic highs are interpreted to coincide with locations of the iron formations and these require ground truthing and follow-up.
6. The Ikanga iron deposit occurs at various depths (0 to over 100 m) in the regolith, scattered, and shows no indication of well defined and concentrated portions in the

subsurface which makes it very difficult to recommend its exploitation until further work and ground truthing is done.

7. The Ikanga iron deposit is a residual deposit derived from a Precambrian banded iron formation (BIF) by chemical weathering processes. Plots of the geochemical data confirm this conclusion. The BIF from which the Ikanga iron deposit is derived occurred in along the Neoproterozoic Mozambique Belt with destruction of primary fabrics correlated as due to prolonged polycyclic deformation and metamorphism.
8. This deposit is considered to be of low economic value until more work is done to prove economic viability. More resources will be required to conduct further tests and to pilot extraction to find out whether this deposit can pay for itself.

5.7 Recommendations

This deposit is a scattered one, and so it requires detailed exploration. The following are the recommendations arising from this study:-

1. That ground truthing and follow-up of the magnetic anomalies be carried out to further define in more detail the nature and extent of the mineralized zone.
2. That soil grids be established at least two hundred meters apart, six hundred meters total as base line and with three intersecting cross traverse lines, each two hundred meters (m) long on either side of the base line perpendicular to it. It is further recommended that two trenches on both sides of each cross line be dug at the spaces of fifty (50) meter (m) intervals for more detailed sampling..
3. The length of each trench should be ten (10) meters (m), width two (2) meters (m), and depth two (2) meters (m). At this depth it is possible to approach the saprocks. Geochemical data will then be collected for analyses in these trenches. This method is less expensive than drilling but labor intensive. This approach will be appropriate since the magnetic method at times does not give a total picture and identity of some iron ore bodies and may yield false anomalies. Following the trenching phase, drilling may then follow to confirm the nature of the magnetic anomalies in the Ikanga area.
4. The soil composition in the study area is also good for bricks making, and can be used for building brick houses. The soil bricks are good because they are rich in iron content which make them hold together. The tenacity of the bricks will give the buildings long life times.

5. Finally it is strongly recommended that geological professionals should conduct further research in the study area to confirm the results of this study as this area definitely has potential for occurrence of economic mineral deposits.

REFERENCES

Albert, C., and McCulloch, M.T., 1993.Rare earth element and neodymium composition of Banded iron formations and associated shales from Hamersley western Australia, *Geochimica et Cosmochimica Acta*, **57**, pp. 187-204.

Anand, R.R.,& Butt, C.R.M., 1988. The terminology and classification of the deeply weathered regolith. Division of Exploration Geoscience, CSIRO, Perth.

Anand, R. R., Smith, R. E., Phang, C., Wildman, J. E., Robertson, I. D., and Munday, T. J., 1993. Geochemical exploration complex lateritic environment of YilgarnCraton, WA.CSIRO, division of exploration and mining. Restricted Report 442 (reissued as open file report 58, CRC LEME, Perth, 1998).

Appel, P.W.U., 1980.On the Early Archaean Isua iron-formation, west Greenland, *Precambrian Research*, **11**, pp. 73-98.

Baker, B. H., 1954. The Geology of Southern Machakos District. Geol. Survey Kenya, Report No. 27.

Beukes, N.J., 1973. Precambrian iron-formations of southern Africa. *Economic Geology*, **68**, pp. 960-1024.

Beukes, N.J., 1983. Paleoenvironmental setting of iron-formations in the depositional basin of the Transvaal Super group, South Africa, *In:*Trendall A.F and Morris R.C. (eds.). *Iron-Formation: Facts and Problems*, Elsevier, New York, pp. 131-209.

Beukes, N.J., and Klein, C., 1992.Models for iron-formation deposition, *In:* Schopf J.W. and Klein C. (Eds.).*The Proterozoic Biosphere, a multidisciplinary study.* Cambridge University Press, New York, pp. 147-152.

Boadi, I.O., 1991. Origin of mega- gold placer deposits in the light of data on Bukon Jideh deposit, Liberia, and on Tarkwa deposit,Ghana.

Bowell, R.J., Gize, A.P., Hoppis, H.A., Laffoley, N.A., and Rex, A.J., 1991. Mineralogical and chemical characteristics of tropical weathering profile in Ghana: Implication for gold exploration in Brazil, Gold 91, E.A Ladeira, ed., pp. 713-714.

Brown, F.H., and McDouglas, I., 2011.Geochronology of the Turkana depression of northern Kenya and southern Ethiopia.*Evolutionary Anthropology*, **20(6)**, pp.217-27. Available at: http://www.ncbi.nlm.nih.gov/pubmed/22170691 [Accessed February 9, 2012].

Butt, C. M., 1988. Genesis of supergene gold deposits in the lateritic regolith of the Yilgarn Block, WA, in *Economic Geology Monograph 6*, the Geology of Gold Deposits: The Perspectives in 1988, pp. 460-470.

Champion, D. E., and Criss, R.E., 1984. Magnetic properties of granitic rocks from the Southern half of the Idaho batholith- influence of hydrothermal alteration and Implications for aeromagnetic interpretation: *Journal of Geophysical Research*, **89**, No. B8 pp.7061-7076.

Clout, J.M. F., 2006.Iron formation hosted iron ores in the Hamersley province of Western Australia, Source: Applied Earth Science, volume 115, No. 4, 2006, pp.115-225 (11).

Condie,K. C., 1981. *Archaean Greenstone Belts*, Elsevier, Amsterdam, 442 pp.

Davy and EL-Ansary., 1989. Some Precambrian banded iron formations (BIFS) from around the world: Their age, geologic setting, mineralogy, metamorphism, geochemistry, and origins, *American Mineralogist*, **90**, No.10, pp. 1473-1475.

Desa, M., Pawangan, D. M., Ramana, M., Ramprasad, M. V., and Shailaja, B., 2007. Geophysical oceanography, National Institute of Oceanography, Dana Paula, Goa-403004, India.

Dodson, R.G., 1955 Geology of the North Kitui Area, Degree Sheet 45, N.W. Quarter, Geol. Survey Kenya, Report No. 33, 27 pp.

Dodson, R.G., 1953. Geology of the South-East Machakos Area. Report No. 25, Geol. Survey Kenya.

Doeky,T.R., 2012. Gold Exploration-Nyanza Solik Project Overview, Kenya. Source: http://www.stockportexploration.com/s/Nyanza.asp.

Dorr, J. V. N., 1964. Supergene iron ores of Minas Gerais, Brazil. *Economic Geology*, **59**, No. 7, 1203-1240.

Dymek, R.F., and Klein, C., 1988. Chemistry, petrology and origin of banded iron formation lithologies from the 3800 Ma Isua supracrustal belt, West Greenland. *Precambrian Research,* **39**, pp. 247-302

Feibel, C.S., 2011. A Geological History of the Turkana Basin. *Evolutionary Anthropology*, 216, pp. 206–216.

Fripp, R.E.P., 1976. Stratabound gold deposits in Archaean banded iron-formation, Rhodesia. *Economic Geology*, **71**, pp. 58-75.

Glossary of Geology, Second Edition, 1980. Edited by Bates, R.L and Jackson, J. A., American Geological Institute, Falls Church, Virginia, 751 pp.

Goodwin, A.M., 1973. Archaean volcanogenic iron-formation of the Canadian shield, *Sci. Terre*, 9, pp. 23-34.

Gross, G.A., 1983. 1983. Tectonic systems and the deposition of iron-formation, *Precambrian Research*, **20**, pp. 171-187.

Griffen, D. T., and Phillips, W.R., 2004. Optical mineralogy, the non-opaque minerals.

Groves, D.I., Phillips, N., Ho, S.E.,Houston, S.M., and Standing, C.A., 1987.Craton-scale distribution of Archaean greenstone gold deposits: predictive capacity of the metamorphic model, *Economic Geology*, **82**, pp. 2045-2058.

Hamade T., Konhauser K.O., Raiswell R., Goldsmith S., Morris R.C., 2003, using Ge/Si Ratios to decouple iron and silica fluxes in Precambrian banded iron formation, *Geology*, **31**, pp. 35-38.

Hanna, W. F., 1969. Negative aeromagnetic anomalies over mineralized areas of the boulder, Batholith, Montana: U.S. Geological Survey Professional Paper 650-D, pp. 159- 167.

Holland, H.D., 1973. The oceans: A possible source of iron in iron formations. Economic *Geology*, **68**, pp. 1169-1172.

Hsu, S. K., 2002. Imaging magnetic sources using Euler's equation, *Geophys. Prosp*. **50**, pp.15-25

Ikanga area Landsat view of band ratios (3:1) for iron oxides. Available at htt/twitter.com/USGSLandsat at images at download for free at: htt/eros.USGS/images gallery/or htt/landsat at look.usgs.gov. Courtesy of Howell, E., 2013).

James, H.L., 1954. Sedimentary facies of iron formation, *Economic Geology*, **49**, pp. 235-293.

James, H.L., and Trendall, A.F., 1982. Iron formation: distribution in time and paleoenvironmental significance, *In:* Holland H.D., Schidlowski M. (eds.), Mineral Deposits and the Evolution of the Biosphere, Springer-Verlag, New York, pp. 199-218.

Joubert, P.,1966. Geology of the Loperot area. Geological Survey of Kenya, Report No. 74, 51 pp.

Kennedy, A., 1989. Southern Cross Mining: A new gold producer in Ghana, *Mining Magazine*, **6/89**, pp. 476-452.

Kimberley, M.M., 1978. Paleoenvironmental classification of iron formations. *Economic Geology*, **73**, pp. 215-229.

Klein, C., 2002. Some Precambrian banded iron formation (BIF) from around the world: Their age, geologic setting, mineralogy, metamorphism, geochemistry, and origin. The *American Mineralogist*, **90**, 1473-1499.

Konhauser, K.., Hamada, T., Raiswell, R., Ferris, F., Southam, G., and Canfield, D., 2002. Could bacteria have formed the Precambrian banded iron formation?. *Geology*, **30**, pp. 1079-1082.

Kuhn, S., Ogola, J., and Sango, P., 1990.Regional Setting and nature of gold mineralization in Tanzania and northwest Kenya. *Precambrian Research*, **46**, 71-82, Amsterdam.

Kuhn, S., 1984. Late Precambrian plate tectonics and orogeny: A need to redefine the term Pan-African. In: Klerky, J. and Michot, J.(Eds), Geologie Africaine- African Geology, 23-28; Tervuren.

L' Vov, B. V., 2005. Fifty years of atomic absorption spectrometry. *J. Anal. Chem*., **60**, pp. 282-392.

Mathu, E.M. 1992. The Mutito and Ikoo faults in the Pan-African Mozambique Belt, Eastern Kenya. In: R. Mason (Editor), Basement Tectonics 7. Kluwer Publishers, The Netherlands, pp. 61-69.

Mathu, E. M., and Tole, M. P., 1984. Geology of the Ikanga Hills Area. *Journ. Afri. Earth Sci*., **2**, pp. 10-16.

Mathu, E.M., Ichang'i D.W. and Dindi, E.W. 1994. The geology, structures and tectonics of the Mozambique belt rocks in Kajiado District, S.W.Kenya. Proceedings of the international Geological Field Conference held in the Mozambique Orogenic belt in East Africa, Arusha, Tanzania (1994). IGCP Project 348 (Extended Abstract)

Morley, C.K., Wescott, W.A., Stone, D.M., Harper, R.M., Wigger, S.T., and Karanja, F.M., 1992. Tectonic evolution of the northern Kenyan rift. *Journal of Geological Society of London*, **149** (Aramboury) 1933, pp. 333-348.

Morris ,R., 1993. Genetic modeling for banded iron formation of the Hamersley Group, Pilbara Craton, western Australia. *Precambrian Research*, **60**, pp. 243-286.

Nyamai, C. M., Mathu, E. M., Wallbrecher, E., and Opiyo-Akech, N. 2003. A reappraisal of the Geology, Geochemistry, Structures, and Tectonics of the Mozambique Belt in Kenya, East of the Rift System. *African Journal of Science and Technology*, **4**, No. 2, pp. 51-71.

Nyamai, C.M., Opiyo-Akech, N., Gaciri, S.J., and Fujimaki, H., 2000. Structures, metamorphism and geochronology of the Mozambique Belt metamorphic and intrusive rocks from Matuu-Masinga area, central Kenya. *African Journal of Science and Technology (AJST), Science and Engineering Series*, **1**, No.1, pp 47-55.

Nyamai, C.M. 1999. Crustal evolution of the Neoproterozoic Mozambique belt rocks in Matuu-Masinga area, central Kenya: Implications to their tectonic setting and potential mineralization. Ph.D Degree Thesis, University of Nairobi, Kenya. 162 pp.

Nyamai, C.M., Opiyo-Akech, N., Gaciri, S.J., and Fujimaki, H. 1999. Geochemistry and Tectonomagmatic affinities of the Mozambique belt intrusive rocks in Matuu-Masinga area, central Kenya. *Gondwana Research* , **2**, pp. 387-399.

Ohmoto, H., and Felder, R. P., 1987.Bacteria activity in the warmer, sulphate-bearing Archaean oceans. *Nature*, **328**, pp. 244-246.

Olang, M.O., 1979. Vegetation covers assessment in Turkana District, Kenya. Kenya Rangeland Econoligical Monitoring Ubit, Nairobi, Kenya, 24 pp.

Patwardhan, A. M., 1999. The dynamic earth system. Prentice-Hall of India, PVT Limited, 416 pp.

Phillips, G.N., Groves, D.I, and Martyn, J.E., 1984. An epigenetic origin for Archaean banded iron-formation-hosted gold deposits. *Economic Geology*, **79**, pp. 162-171.

Piper, J. D. A., 1974.Proterozoic crustal distribution, mobile belts and apparent polar movement. *Nature*, **251**, pp. 381-384.

Piper, J. D. A., 1975.Proterozoic supercontinent: Time duration and the Greenville problem. Nature, 256, pp. 519-520. Piper, J. D. A., 1976.Paleomagnetic evidence for Proterozoic supercontinent. *Phil. Trans. R. Soc. Lond*., **A230**, 469-9.

Reid, A.B., Allsop, J.M., Granser, H., Millet, A. J., and Somerton, I. W. (1990), Magnetic interpretation in three dimensions using Euler deconvolution, *Geophys.*, **55**, pp. 80-91.

Reynold, R. L., Rosenbaum, J. G., Hudson, R. M., and Fishman, N. S., 1990. Rock magnetism, the distribution of magnetic minerals in the earth's crust, and aeromagnetic anomalies; In Hanna, W. F., ed., geologic application of modern aeromagnetic surveys: U.S. Geological Survey Bulletin 1924, pp. 24-45.

Rop, B.K., 2011. Hydrocarbon Characteristics of source rocks in Loperot-1 Well, Northwest Kenya. *Proceedings, Kenya Geothermal Conference, 2011.*

Satellite imagery of the study area. Source: Htt/twitter.com/USGS Landsat images at download for free at: htt/eros.USGS.gov/image gallery/or htt//landsatlook.usgs.gov, courtesy of Howell, 2013).

Sanders, L.D. 1954. Geology of the Kitui Area, Degree Sheet 53, N.W. Quadrant. Geol. Surv. Kenya, Report No. 30, 53 pp.

Saggerson, E.P. 1957. Geology of the South Kitui Area, Degrees Sheet 53, South West Quarter. Geol. Surv. Kenya, Report No. 37, 49 pp.

Schlüter, T., 1997. Geology of East Africa, Gebrüder Borntraeger. Berlin, Stuttgart, 484 pp.

Schoeman, J.J., 1948. A geological reconnaissance of the area west of Kitui Township. Geol. Surv. Kenya, Report No. 14, 43 pp.

Shackleton, R. M., 1986. Precambrian collision tectonics in Africa. In: Coward, M. P., & Res, A. C.,, (Ed). Collision tectonics, pp. 329-349. Blackwell; Oxford.

Simonson, B.M., 1985. Sedimentological constraints on the origins of Precambrian iron formation. *Geological Society of America Bulletin*, **96**, pp. 244-252.

Smith, R. E.,Anand, R. R., and Alley, N. E., 2000. Use and application of paleo-weathering Surfaces in mineral exploration in Australia. *Ore Geology Reviews*, **16**, pp.185-204.

Straaten, H.P.Van., 1984. Contribution to the Geology of the Kibaran Belt in northwest Tanzania. UNESCO Geol. Development. Newsletter 3, 59-68, Paris, Nairobi.

Topographical Map of Ikanga. Source: D.O.S 423(Series Y731), Edition I-D.O.S., Published by the Directorate of Oversea Surveys for the Kenya Government, Sheet 164/1, 1965.

Turner, F., J., 1948.Mineralogical and structural evolution of the metamorphic rocks. *Geol. Soc. America Memoir*, **30**.

Veizer, J., 1983.Geologic evolution of the Archaean-Early Proterozoic Earth, *In:* Schopf J.W. (ed.), Earth's Earliest Biosphere, Princeton University Press, New Jersey, pp. 240-259.

Walsh, A., 1955. The application of atomic absorption spectra to chemical analysis, *Spectrochim Acta*, **7**, 108-117.

Walsh, J., 1959. The Geology of Ikutha Area, Degree Sheet No 60, N.W. Quarter. Geological Surv. Kenya, Report No.56, 37 pp.

Warden, A.J. and Horkel, A.D., 1984. The Geological Evolution of the NE Branch of the Mozambique Belt (Kenya, Somalia, Ethiopia), *Mitteilungen Der Oesterreichischen Geologische Gesellschaft*, **77**, pp. 161-184.

Windley, B.F. 1984. The Evolving Continents. 2nd Edition Wiley, London, 420 pp.

APPENDIX

The following sections are appendix. Magnetic data acquired during the ground geophysical mapping in the field are presented

Appendix : Magnetic data from Ikanga area

X (UTM)	Y (UTM)	Total Field (nT)
393381	9817014	33598
393952	9817014	33573
393971	9817028	33581
393989	9817040	33583
393900	9817005	33568
393922	9817020	
393941	9817031	33580
393955	9817044	33573
393963	9817070	33502
393976	9817093	33580
393993	9817119	33591
393853	9817011	33579
398544	9	33584

	81702 6	
393825	981704 1	33573
393908	981705 6	33714
393940	981707 3	33572
393924	981709 0	33583
393938	981710 3	33597
393953	981711 7	33558
393969	98	33577

	17128	
393905	981714 1	33581
394010	981715 6	33584
393930	981701 9	33580
393768	981703 2	33615
393723	981704 6	33558
393800	981706 0	33614
393813	981	33521

	7074	
393827	9817088	33597
393842	9817098	33609
393856	9817113	33594
393870	9817188	33600
393886	9817140	33558
393902	9817153	33607
393918	98117	33611

	169	
393933	9817185	33602
393945	9817198	33592
393961	9817226	33589
393975	9817226	33600
393989	9817240	33613
X (UTM)	Y (UTM)	Total Field (nT)
394002	98172	33587

	51	
394012	9817258	33594
393648	98170002	33621
393680	98170555	33674
393695	98170772	33653
393708	98170889	33530
393718	98171106	33537
393727	98171712	33582

	6	
393747□9817162 9817162	335823 3582	□393764□981719 9 393764
393800□9817211 9817211	335873 3587	□393816□9817226 393816
393825	98172466	33592
393838	98172577	33604
393857	98172668	33670
393877□9817280 9817280	335744 3574	□393893□9817293 393893
393914	98173044	33584
393933□9817315 9817315	335899 3589	□393902□9817326 393902

393969□9817336 9817336	3 3 5 8 1	□393987□9817346 393987
394006□9817353 9817353	3 3 5 7 6	□394022□9817361 394022
393561	9 8 1 7 8 0 0	33630
393574	9 8 1 7 0 1 6	33616
393588□9817031 9817031	3 3 5 9 1	□393601□9817068 393601
393609□9817063 9817063	3 3 5 9 1	□393622□9817082 393622
393685	9 8 1 7 1 6 9	33432
393699	9 8 1 7 1 8 6	32132
393716	9 8	33480

	1 7 2 0 3	
394034□9817461 9817461	3 3 4 5 2	□393737□9817231 393737
(UTM)	Y (U T M)	Total Field (nT)
393751	9 8 1 7 2 5 0	33526
393755	9 8 1 7 2 5 4	33519
393771	9 8 1 7 2 6 9	33509
393786	9 8 1 7 2 8 6	33516
393811	9 8 1 7 3	33507

	00	
393818	98173144	33529
393830	98173229	33624
393845	98173448	33525
393862	98173553	33519
393880	98173666	33523
393900	98173779	33523
393917	98173939	33522

	0	
393935	98174002	33474
393961	98174111	33496
393977	98174225	33518
393994	98174447	33515
393014	98174668	33518
394035	98174600	33505
393461	98170009	33581

393477	98170111	33601
393497	98170226	33604
393512	98170444	33583
393527	98170559	33588
393546	98170777	33567
393556	98170889	33582
393571	98171006	33589
393586	9	33578

	81712121	
393602	98171737	33594
393614	98171747	33809
393625	98171768	33581
393693	98172243	33481
393705	98172256	33474
393717	98172273	33471
393724	98	33480

	17288	
393732	9817305	33389
393744	9817323	33450
393750	9817344	33518
393762	9817365	33530
393770	9817375	33470
393786	9817393	33496
393803	981	33511

	7404	
393820	9817414	33522
393833	9817429	33528
X (UTM)	Y (UTM)	Total Field (nT)
393846	9817444	33518
393862	9817457	33496
393882	9817465	33512
393898	9817	33519

	476	
393919	9817482	33522
393929	9817490	33528
393944	9817501	33532
393962	9817511	33524
393976	9817522	33516
393992	9817530	33494
394004	981775	33505

	47	
393998	9817551	33531
393353	9817001	33648
393368	9817011	33681
393378	9817023	33680
393391	9817039	33626
393408	9817053	33608
393419	981706	33662

	4	
393433	9817080	33611
393448	9817094	33621
393465	9817109	33599
393479	9817123	33588
393495	9817140	33582
393509	9817155	33576
393525	9817171	33573
393537	9817184	33567
393549	9817195	33562
393561	9817210	33553
393572	9817223	33560
393591	9817238	33562
393607	9817252	33546
393623	9817271	33548
393690	9	33524

	8173333	
393699	9817352	33502
393713	9817664	33539
393728	9817378	33493
393746	9817391	33463
393760	9817407	33351
393772	9817422	33604
393786	98	33506

	174335	
393804	9817449	33524
393820	9817463	33497
393837	9817477	33536
X (UTM)	Y (UTM)	Total Field (nT)
393852	9817488	33525
393869	9817250	33453
393880	981	33521

	7 5 1 2	
393896	9 8 1 7 5 2 6	33514
393609	9 8 1 7 5 4 6	33517
393920	9 8 1 7 5 6 1	33524
393937	9 8 1 7 5 7 7	33521
393947	9 8 1 7 5 8 8	33530
393964	9 8 1 7 6 0 3	33540
393979	9 8 1 7	33531

	6 2 4	
393989	9 8 1 7 6 3 8	33526
393997	9 8 1 7 6 5 1	33532
393254	9 8 1 7 0 0 1	33622
393273	9 8 1 7 0 1 7	33672
393289	9 8 1 7 0 3 0	33689
393302	9 8 1 7 0 4 0	33669
393314	9 8 1 7 0	33516

	54	
393329	98170666	33736
393341	98170800	33607
393354	98170997	33610
393367	98171112	33567
393373	98171311	33536
393389	98171142	33477
393408	98171715	33482

	7	
393419	98171711	33491
393437	98171784	33516
393449	98171795	33523
393462	98172207	33521
393472	98172220	33534
393490	98172332	33521
393507	98172249	33529

393522	9817265	33514
393536	9817279	33519
393551	9817295	33507
393565	9817311	33517
393581	9817328	33464
393590	9817764	33550
393604	9817359	33531
393684	9	33441

	817437	
393698	9817452	33536
393712	9817464	33518
393730	9817477	33433
393746	9817490	33397
X (UTM)	Y (UTM)	Total Field (nT)
393761	9817502	33469
393777	98	33445

	1 7 5 1 8	
393795	9 8 1 7 5 3 0	33483
393810	9 8 1 7 5 4 4	33482
393821	9 8 1 7 5 5 9	33488
393843	9 8 1 7 5 7 5	33481
393858	9 8 1 7 5 9 0	33483
393876	9 8 1 7 5 9 0	33484
393892	9 8 1	33500

	7 6 0 6	
393912	9 8 1 7 6 4 0	33500
393925	9 8 1 7 6 5 6	33501
393937	9 8 1 7 6 6 9	33501
393953	9 8 1 7 6 8 3	33500
393964	9 8 1 7 6 9 9	33498
393974	9 8 1 7 7 1 8	33506
393986	9 8 1 7	33505

	738	
393996	9817768	33502
393151	9817000	33651
393168	9817014	33665
393180	9817024	33630
393196	9817038	33692
393209	9817051	32765
393224	981770	32634

	64	
393239	9817078	32986
393252	9817092	33379
393258	9817102	33439
393268	9817118	33460
393278	9817134	33434
393293	9817153	33414
393305	981716	33450

	4	
393325	9817179	33253
393335	9817194	33347
393350	9817210	33605
393366	9817223	33605
393377	9817236	33449
393397	9817250	33400
393406	9817266	33381
393419	9817280	33431
393434	9817300	33372
393447	9817316	33376
393461	9817332	33419
393477	9817346	33500
393492	9817339	33417
X (UTM)	Y (UTM)	Total Field (nT)
393508	9	33419

	8173776	
393522	98173933	33422
393539	98174009	33425
393555	98174224	33430
393564	98174335	33431
393588	98174447	33427
393595	98174622	33429
393683	98	33542

	1754343	
393701	98175761	33367
393716	98175772	33339
393733	98175885	33271
393760	98178996	33322
393769	98173662	33276
393775	98176227	33341
393787	981	33401

	7645	
393798	98176556	33362
393815	98176669	33303
393835	98176884	33413
393851	98176998	33433
393865	98177005	33445
393877	98177333	33521
393892	98177	33454

	760	
393909	98177766	33454
393924	98177778	33451
393939	98177793	33461
393955	98178009	33460
393969	98178226	33456
393977	98178446	33461
393982	98178	33453

	55	
39400	9817664	33459
393058	98170000	32860
393058	98170211	32823
393092	98170361	32761
393105	98170488	32690
393119	98170600	33428
393133	98170707	32554

	6	
393148	98170900	32562
393165	98171009	32437
393182	98171125	32620
393196	98171411	32651
393210	98171555	32733
393225	98171669	32650
393238	98171855	32401

X (UTM)	Y (UTM)	Total Field (nT)
393253	9817208	32752
393266	9817223	33134
393279	9817238	33221
393293	9817255	33256
393309	9817274	33320
393322	9817293	33014
393339	9817311	33228
393349	9817321	33391
393364	9817338	33271
393377	9817348	33288
393405	9817348	33246
393417	9817398	33264
393439	9817425	33275
393459	98	33317

	17447	
393475	9817464	33374
393495	9817848	33353
393513	9817499	33363
393528	9817517	33374
393548	9817536	33390
393567	9817563	33383
393595	981	33394

	7505	
393677	9817662	33393
393694	9817679	33313
393712	9817697	33314
393734	9817719	33570
393758	9817732	33418
393778	9817751	33399
393800	9817	33398

	773	
393815	9817789	33449
393827	98178005	33446
393843	98178222	33445
393854	98178339	33458
393871	98178667	33468
393889	98178881	33478
393910	9817878	33469

	98	
393926	98179166	33483
393900	98180000	33257
393882	98179855	33450
393869	98179677	33448
393855	98179500	33464
393843	98179377	33440
393829	9817922	33450

	4	
393815	9817909	33435
X (UTM)	Y (UTM)	Total Field (nT)
393799	9817893	33421
393782	9817877	33378
393766	9817863	33590
393747	9817842	33392
393723	9817822	33071

393706	9817802	33307
393690	9817787	33406
393673	9817775	33396
393656	9817759	33414
393639	9817741	33514
393566	9817661	33625
393549	9817651	33326
393533	9	33314

	8176338	
393523	98176227	33306
393499	98176111	33242
393480	98175888	33267
393464	98175733	33255
393442	98175558	33209
393418	98175311	33201
393398	98	33183

	175007	
393381	9817490	33130
393364	9817474	33127
393347	9817454	33118
393333	9817439	33025
393320	9817423	32590
393204	9817405	33103
393289	981	33033

	7388	
393272	98173673	32844
393257	98173493	32707
393239	98173293	32194
393222	98173466	32453
393206	98172888	32107
393193	98172722	32290
393173	98177	32172

	251	
393150	98172288	32306
393131	98172088	32804
393109	98171789	32719
393031	98171745	32771
393076	98171760	32834
393052	98171734	32800
393032	98171711	32848

	15	
393014	9817098	32904
392999	9817079	32846
X (UTM)	Y (UTM)	Total Field (nT)
392984	9817058	32825
390297	9817035	32902
392964	9817014	32857
392956	9817000	32902

	0	
392843	9817000	33357
392859	9817012	33302
392879	9817035	33224
392896	9817048	33156
392928	9817064	33096
392953	9817089	33149
392975	9817109	32912

393005	9817139	33048
393022	9817152	32967
393049	9817179	32053
393061	9817199	32747
393080	9817218	32582
393096	9817237	32454
393118	9817251	32256
393131	9	32193

	8172261	
393157	9817277	32334
393180	9817295	32453
393195	9817305	32077
393219	9817343	32080
393235	9817363	32675
393255	9817386	32510
393282	98	32634

	1 7 4 1 7	
393303	9 8 1 7 4 4 1	33276
393328	9 8 1 7 4 5 3	32775
393330	9 8 1 7 4 8 2	33029
393370	9 8 1 7 5 0 1	33123
393393	9 8 1 7 5 2 7	33101
393401	9 8 1 7 5 5 2	33090
393421	9 8 1	33090

	7 5 5 7	
393452	9 8 1 7 6 0 0	33190
393473	9 8 1 7 6 2 0	33214
393499	9 8 1 7 6 4 5	33232
393522	9 8 1 7 6 6 9	33252
393542	9 8 1 7 6 9 0	33277
393562	9 8 1 7 7 0 4	33288
393598	9 8 1 7	33315

	7 2 0	
393660	9 8 1 7 8 0 5	33367
393677	9 8 1 7 8 2 5	33381
393705	9 8 1 7 8 5 2	33353
X (UTM)	Y (U T M)	Total Field (nT)
393727	9 8 1 7 8 8 0	33311
393753	9 8 1 7 9 0 9	33442
393766	9 8 1 7 9	33284

	3 0	
393777	9 8 1 7 9 5 6	33319
393795	9 8 1 7 9 8 5	33337
393803	9 8 1 8 0 0 0	33379
392755	9 8 1 7 0 1 2	33476
392772	9 8 1 7 0 2 6	33909
392782	9 8 1 7 0 3 4	33799
392799	9 8 1 7 0 4	33679

	5	
392815	9817058	33604
392826	9817072	33434
392858	9817085	33493
392874	9817095	33483
392902	9817113	33062
392920	9817125	33069
392941	9817141	33747
392955	9817150	32883
392964	9817161	32906
392981	9817173	32791
392998	9817178	32773
393006	9817194	32681
393019	9817205	32274
393036	9817225	32781
393059	9	32694

	8172 37	
393978	98172 54	32624
393102	98172 70	32636
393124	98172 89	32419
393143	98173 00	32386
393160	98173 14	32303
393187	98173 39	32112
393203	98	32263

	17 368	
393219	98173 87	32112
393240	98174 06	32027
393281	98174 29	32608
393277	98174 45	32795
393293	98174 62	32971
393310	98174 84	32899
393334	981	32990

	7509	
393354	9817530	32972
393374	9817551	33601
393391	9817584	33146
393423	9817610	33180
X (UTM)	Y (UTM)	Total Field (nT)
393445	9817636	33186
393477	98117	33249

	657	
393500	9817677	33273
393525	9817293	33315
393547	9817715	33324
393563	9817731	33334
393581	9817752	33362
393603	9817764	33372
393667	98178	33428

	64	
393686	98178855	33402
393692	981790909	33416
393706	981793938	33416
393725	981797974	33386
393738	981799955	33405
393699	981700011	33311
393559	981790900	33323

	2	
393541	98178881	33335
393513	98176822	33312
393484	98178334	33283
393455	98178111	33239
393431	98177795	33192
393408	98177733	33231
393480	98177764	33184

393362	9817746	33153
393342	9817722	32928
393309	9817702	32830
393208	9817692	32692
393274	9817670	32825
393247	9817648	32499
393222	9817628	32270
393193	9	32260
	817603	
393171	9817578	32027
393146	9817552	32425
393127	9817532	32358
393105	9817511	32527
393090	9817495	32613
393062	9817476	32607
393030	98	32505

	1745 0	
393013	9817 433	32500
392940	9817 422	32603
392952	9817 379	33442
392934	9817 374	32759
392894	9817 331	32767
X (UTM)	Y (U T M)	Total Field (nT)
392876	981	32987

	7314	
392846	9817 286	32929
393821	9817 260	33053
392800	9817 244	33438
392778	9817 223	33218
392752	9171 96	33683
393736	9817 174	33691
X (UTM)	Y (U	Total Field (nT)

	TM)	
392725	9817153	33753
392707	9817128	33634
392692	9817148	33672
392673	981	33975

	7076	
392651	98170005	33842
392636	98170200	33795
392636	98170000	33716